TITLE: Tailored First- and Second-Line CDK4-Targeting Treatment Combinations in Mouse Models of Pancreatic Cancer

AUTHORS: Angela Chou[1,2,3], Danielle Froio[1], Adnan M Nagrial[1,4], Ashleigh Morgan[1], Kendelle J Murphy[1], Venessa T Chin[1], Dalia Wohl[1], Angela Steinmann[1], Rhys Stark[1], Alison Drury[1], Stacey N Walters[1], Claire Vennin[1], Andrew Burgess[1,2], Mark Pinese[1], Lorraine A Chantrill[1,5], Mark Cowley[1], Timothy J Molloy[6], Australian Pancreatic Cancer Genome Initiative (APGI)*, Nicola Waddell[7], Amber Johns[1], Sean M Grimmond[8], David K Chang[9,10], Andrew V Biankin[9,10], Owen J Sansom[11], Jennifer Morton[11], Shane T Grey[1,2], Thomas R Cox[1], John Turchini[12,13,14], Jaswinder Samra[15], Stephen J Clarke[12], Paul Timpson[1,2], Anthony J Gill[1,12,13,14] and Marina Pajic[1,2**].

AFFILIATIONS: [1]The Kinghorn Cancer Centre, The Garvan Institute of Medical Research, 384 Victoria St, Darlinghurst, Sydney, NSW 2010, AUSTRALIA; [2]St Vincent's Clinical School, Faculty of Medicine, University of NSW, AUSTRALIA; [3]Department of Anatomical Pathology SYDPATH, Darlinghurst, Sydney, NSW 2010, AUSTRALIA; [4]Crown Princess Mary Cancer Centre, Westmead Hospital, Sydney, NSW 2145, AUSTRALIA; [5]St. Vincent's Hospital, 370 Victoria Street, Darlinghurst, NSW 2010; AUSTRALIA; [6]St Vincent's Centre for Applied Medical Research, 405 Liverpool St, Darlinghurst, NSW 2010, AUSTRALIA; [7]Department of Genetics and Computational Biology, QIMR Berghofer Medical Research Institute, Herston, QLD 4006, AUSTRALIA; [8]University of Melbourne, Parkville, VIC 3010, AUSTRALIA; [9]Wolfson Wohl Cancer Research Centre, Institute of Cancer Sciences, University of Glasgow, Bearsden, Glasgow, Scotland G61 1BD, UNITED KINGDOM; [10]West of Scotland Pancreatic Unit, Glasgow Royal Infirmary, Glasgow, Scotland G4 OSF,

UNITED KINGDOM; [11]Cancer Research UK Beatson Institute, Institute of Cancer Sciences, University of Glasgow, Glasgow, UNITED KINGDOM; [12]Sydney Medical School, University of Sydney, NSW 2006, AUSTRALIA; [13]Department of Anatomical Pathology, Royal North Shore Hospital, St Leonards, Sydney, NSW 2065, AUSTRALIA; [14]Cancer Diagnosis and Pathology Research Group, Kolling Institute of Medical Research, St Leonards, NSW 2065, AUSTRALIA; [15]Department of Surgery, Royal North Shore Hospital, St Leonards, Sydney, NSW 2065, AUSTRALIA.

*See supplementary information 1 for consortium details.

CORRESPONDING AUTHOR:

Dr Marina Pajic,

Personalized Cancer Therapeutics Group

Cancer Division

The Garvan Institute of Medical Research

370 Victoria St Darlinghurst NSW 2010

Phone: +61 2 93555834

Fax: +61 2 93555868

Email: m.pajic@garvan.org.au

WORD COUNT: *excluding title page, abstract, references, figures and tables.*

4,024

ABSTRACT

Objective: Extensive molecular heterogeneity of pancreatic ductal adenocarcinoma (PDA), few effective therapies and high mortality make this disease a prime model for advancing development of tailored therapies. The p16-cyclin D-CDK4/6-retinoblastoma protein (CDK4) pathway, regulator of cell proliferation, is deregulated in PDA. Our aim was to develop a novel personalized treatment strategy for PDA based on targeting CDK4.

Design: Sensitivity to potent CDK4/6 inhibitor PD-0332991 (palbociclib) was correlated to protein and genomic data in 19 primary patient-derived PDA lines to identify biomarkers of response. *In vivo* efficacy of PD-0332991 and combination therapies was determined in subcutaneous, intrasplenic and orthotopic tumor models derived from genome-sequenced patient specimens and genetically-engineered model. Mechanistically, mono- and combination therapy was investigated in context of tumor cell and extracellular matrix (ECM) signaling. Prognostic relevance of companion biomarker, retinoblastoma protein, was evaluated and validated in independent PDA patient cohorts (> 500 specimens).

Results: Subtype-specific *in vivo* efficacy of PD-0332991-based therapy was for the first time observed at multiple stages of PDA progression: primary tumor growth, recurrence (2nd line therapy) and metastatic setting, and may potentially be guided by a simple biomarker (retinoblastoma protein). PD-0332991 significantly disrupted surrounding ECM organization, leading to increased quiescence, apoptosis, improved chemosensitivity, decreased invasion, metastatic spread and PDA progression *in vivo.* Retinoblastoma protein is prevalent in primary operable and metastatic PDA and may present a promising predictive biomarker to guide this therapeutic approach.

Conclusion: This study demonstrates the promise of CDK4 inhibition in PDA over standard therapy when applied in a molecular subtype-specific context.

Keywords: pancreatic cancer, extracellular matrix, tailored therapy

SIGNIFICANCE OF THIS STUDY

What is already known about the subject?

- Despite significant recent efforts into developing novel therapeutics, chemotherapy remains the standard-of-care for patients with advanced pancreatic cancer, despite only modestly improving overall survival.
- We and others have previously shown that pancreatic cancer is a molecularly varied disease, and requires development of personalised treatment strategies to improve survival rates.
- Pancreatic cancer harbors frequent deregulation of the p16-cyclin D-CDK4/6-retinoblastoma protein pathway (CDK4 pathway), which could be therapeutically exploited.

What are the new findings?

- Using a range of robust patient-derived xenograft and cell line models, as “avatars of matched patient pancreatic tumors”, we show exquisite sensitivity to CDK4/6 inhibitor- combinations over standard therapy in subtypes of pancreatic cancer, associated with increased apoptosis, quiescence and reduced expression of markers associated with pancreatic stellate cell activity.

- PD-0332991 facilitates remodeling of the ECM to improve therapeutic efficacy of gemcitabine in a subtype-specific manner and at multiple stages of disease progression: primary tumor growth, recurrence (2^{nd} line therapy) and the metastatic setting, and may potentially be guided by a simple, clinically-applicable biomarker (RB protein).
- CDK4 inhibitor, PD-0332991 (palbociclib) hinders metastatic colonization in the liver while sensitizing cells to shear stress, commonly experienced by metastasizing circulating tumor cells (CTCs), an additional way in which CDK4 inhibition can directly impinge on metastasis in RB-high PDA.
- RB protein expression was identified as an independent prognostic factor for patient survival in two independent patient cohorts of pancreatic cancer and can be detected in a significant proportion of metastatic cases (67%). RB expression correlated between primary and matched metastatic human tissue.
- CDK4 pathway inhibition alone or in combination with chemotherapy leads to multifaceted global inhibitory effects on tumor cells at different stages of PDA progression and reduction in key components within the tumor microenvironment (extracellular matrix), which collectively drive cancer cell proliferation, invasion and chemoresistance.

How might it impact on clinical practice in the foreseeable future?

- Our findings, together with the recent clinical evidence on the efficacy of PD-0332991 in the treatment of breast cancer, support the further clinical companion-biomarker driven development of PD-0332991 as pancreatic cancer therapy, particularly in combination with chemotherapeutic, gemcitabine.

- The use of a tissue-based assay for RB expression could be adapted for clinical application in diagnostics. As high RB expression was detected in a significant proportion of patients with pancreatic cancer (~65%, ~43%, and 67% in cohorts of primary operable and metastatic PDA examined), it may enable stratification and enrichment for the potential responders to the CDK4/6 combination therapy.
- These findings are timely and may be complementary and of direct relevance to the current non-biomarker driven clinical trials testing PD-0332991 in pancreatic and other solid cancers (NCT02501902, NCT03065062).

INTRODUCTION

Pancreatic ductal adenocarcinoma (PDA) is a molecularly diverse disease, driven by aberrations in at least 10 core signaling pathways.[1-4] In addition to revealing new biological insight into the molecular pathogenesis of PDA, these studies have created significant opportunities to develop novel, tailored treatments, as we have recently shown.[5 6] The standard-of-care chemotherapeutic gemcitabine,[7] in combination with nanoparticle albumin-bound paclitaxel (nab-paclitaxel),[8] or FOLFIRINOX (oxaliplatin, irinotecan, fluorouracil and leucovorin)[9] offer only modest increases in patient survival in unselected populations.[10] Selective measures to personalize treatment in this aggressive disease are therefore urgently required.

The p16-cyclin D-CDK4/6-retinoblastoma protein pathway (CDK4 pathway) promotes G_1/S-phase transition and is one of the key signaling pathways deregulated in PDA.[1 2 11] Cyclin D complexes with cyclin-dependent kinases (CDKs) 4 and 6, driving retinoblastoma protein (RB) phosphorylation and G_1 phase progression.[12] In cancer, CDK4 activity and subsequent uncontrolled proliferation can be enhanced by homozygous deletion of *CDKN2A* gene (which encodes $p16^{INK4A}$ protein), CDK4/6 mutations and/or Cyclin D1 (*CCND1*) over-expression or amplification.[13]

Discovery of Cyclin D/CDK4 as an oncogene has fueled development of small-molecule CDK inhibitors (CDKi). Selective CDK4/6i, including PD-0332991 (palbociclib), are showing great potential in the treatment of ER+/HER2- metastatic breast cancer.[14-16] Although no biomarker of treatment response has been found, a key requirement for sensitivity to CDK4/6i in breast cancer may be linked to ER-positivity and dependence of the ER+ subtype on cyclin D1 signaling, enhancing CDK4/6 activity to drive proliferation.[12 17]

In PDA, short-term anti-proliferative activity of CDK4/6i has been described.[18] Here, we investigated the therapeutic efficacy of CDK4/6i and clinically-applicable combinations with long-term follow-up in realistic advanced preclinical patient-derived and genetically-engineered models of PDA. We reveal a new role of CDK4 inhibition in regulating primary tumor growth and stromal desmoplasia in several independent mouse models of RB-high PDA, impairing colonization of secondary sites (liver) and resistance to shear stress, frequently experienced by circulating tumor cells (CTCs), while delaying disease progression in metastatic RB-high PDA. Detailed analyses reveal a complex mechanism of action with PD-0332991 exerting dual effects on both tumor cells and the surrounding environment. Assessment of RB expression, candidate CDK4/6i companion biomarker, revealed high prevalence in primary operable and metastatic human PDA. Collectively, these preclinical findings may offer promising new opportunities in subtype-specific targeting of primary and metastatic PDA.

METHODS

Patient-Derived Models

Our Kinghorn Cancer Centre (TKCC) patient-derived xenografts (PDXs; *n*=45) and patient-derived cell lines (PDCLs; *n*=19) have previously been whole genome sequenced.[1] PDCLs were confirmed by STR profiling as unique (cellbankaustralia.com). Culture conditions, fluorescent ubiquitination-based cell cycle indicator (FUCCI) and luciferase introduction into PDCLs and associated *in vitro* studies: cell cycle, migration, invasion, shear stress, contraction and apoptosis assays are detailed in supplementary information 2.

Animal Studies

In vivo experiments were approved by Garvan/St Vincent's Animal Ethics Committee (14/11, 14/12). Survival studies were performed by subcutaneously implanting early 3rd-passage PDX pieces (~4mm^3) into immunocompromized Balb/c-Fox1nuAusb (Nude) mice. PD-0332991, gemcitabine and nab-Paclitaxel dosages were based on published studies,[5 18 19] with treatment schedules, response measurement and set up for intrasplenic and orthotopic studies detailed in supplementary information 2.

Patient Materials and Immunohistochemistry

Patient samples and data were acquired through the Australian Pancreatic Genome Initiative (APGI)/ International Cancer Genome Consortium (*n*=200), New South Wales Pancreatic Cancer Network (NSWPCN; *n*=365) and the Royal North Shore Hospital metastatic cohort (RNSH; *n*=54), as described.[1 5 20] Ethics approval for acquisition of data and biological material was obtained from human research ethics committees from each participating institution (Sydney Local Health District Human

Research Ethics Committee X11-0220), with further cohort description and immunohistochemical procedures outlined in supplementary information 2.

Statistics

Statistical analyses were performed using GraphPad Prism (V7.0.1, GraphPad, USA) and Statview (V5.0). Correlation analyses were performed using Pearson correlation coefficient test. Comparison between clinico-pathological correlates was performed using Fisher exact, Student *t*- and Chi-squared tests where appropriate. Survival analyses were performed using the log-rank test. For multiple treatment group comparisons significance was determined by One-way ANOVA, followed by Tukey *post hoc* multiple comparisons test where *p<0.05, **p<0.01, ***p<0.001, ****p<0.0001. Clinicopathological variables shown by univariate analysis to have p<0.25 were entered into a Cox proportional hazards regression model for multivariate analysis. To assess the agreement of RB status between primary and metastatic PDAs, Cohen's Kappa and 95% confidence intervals were reported.

RESULTS

PD-0332991 Sensitivity of Pancreatic Cancer Patient-Derived Cell Lines (PDCLs) Correlates with High Levels of Total and Phosphorylated RB Protein

To systematically examine efficacy of CDK4/6i PD-0332991 in PDA, we determined its toxicity in 19 whole genome-sequenced[5] primary PDCLs, and compared these data to several clinically-used chemotherapeutics (supplementary table S1). PDCLs exhibited a broad range of PD-0332991 sensitivity (IC_{50} range 8nM-35μM), with a subset (26%) being highly sensitive (IC_{50}<1μM). The "Genomics of Drug Sensitivity in Cancer" (Wellcome Trust) database analysis revealed an association between *RB1* mutations and pan-cancer PD-0332991 resistance ($P=3.3x10^{-17}$, supplementary figure S1A). As *RB1* mutations in pancreatic cancer are rare[1] (1/19 PDCLs; supplementary table S1), we next correlated the baseline protein expression of key G_1/S checkpoint components (supplementary figure S1B, supplementary table S2) with *in vitro* PD-0332991 response. Of note, total and phosphorylated RB (pRB; Ser780) levels were the most significant biomarkers predicting PD-0332991 sensitivity (figure 1A; r=-0.751; p=0.0002 and r=-0.728, p=0.0004, respectively), with no correlation between G_1/S checkpoint mutations/expression and response to PD-0332991 or chemotherapeutics in pancreatic PDCLs (supplementary table S3, supplementary figure S1C-E).

Effective target modulation was confirmed in candidate RB-high PDCLs by western blotting for pRB post-PD-0332991 treatment (TKCC-03/-05; figure 1B), with no effect in RB-negative PD-0332991-resistant TKCC-27 cells (figure 1B, *right*). Interestingly, in RB-high, p16-positive, *CDK*6-amplified TKCC-26, pRB was reduced post-PD-

0332991, suggesting that in PDA *CDK*6 amplification may support sensitivity to CDK4/6i, irrespective of p16 expression.

Chemotherapeutic Gemcitabine synergizes with PD-0332991 in RB-High and *CDK6*-Amplified Pancreatic PDCLs

Combining PD-0332991 with standard-of-care therapy in PDA, gemcitabine[7], in PDCLs and primary murine PDA cells (figure 1C) from the genetically-engineered Pdx1-Cre, LSL-Kras$^{G12D/+}$, LSL-Trp53$^{R172H/+}$ (KPC) model[21 22] produced robust cell line-specific efficacy, with combination index (CI) analysis[23] showing a synergistic interaction between gemcitabine and PD-0332991 in RB-high PDCLs (TKCC-03,-05,-15,-17,-26; figure 1D) and antagonism in RB-low/negative PDCLs (TKCC-06,-16,-23 and -27) and KPC cells (figure 1E). The robustness of synergy was confirmed by examining gemcitabine/PD-0332991 treatment with 25 drug combinations tested on five PDCLs, with synergy repeatedly observed across variable drug ratios in RB-high and antagonism in RB-low/negative lines (figure 1D,E *inset,* supplementary figure S2).

PD-0332991-based Mono- and Combination Therapies Induce Critical Effects on RB-high Tumor Cells

To understand the cellular mechanism of anti-tumor activity of PD-0332991 and its synergy with gemcitabine, we examined the effect of selected treatments on cell cycle and apoptosis in candidate RB-high/RB-negative PDCLs (figure 1F) transduced with FUCCI, a fluorescent, two-color biosensor of cell cycle progression[24] (supplementary figure S3). Biosensor function and target modulation was confirmed by live cell imaging of PD-0332991-treated FUCCI-PDCLs (supplementary figure S4), showing robust G_0/G_1 arrest specifically in RB-high TKCC-05, not in RB-negative TKCC-27 cells, confirmed by traditional analysis (supplementary figure S4E,F).

Next, PD-0332991 treatment of FUCCI-TKCC-05 significantly induced apoptosis (4-10 days; $p<0.0001$ and $p<0.01$, respectively; figure 1G, supplementary figure S5). In agreement with published work,[25] gemcitabine stimulated apoptosis. Importantly, gemcitabine/PD-0332991 combination significantly increased the apoptotic effect of each monotherapy (figure 1G, supplementary figure S5C,E,G), not observed in RB-negative TKCC-27 (figure 1H, supplementary figure S5D,F,H), supporting the potentially cytotoxic mechanism of action of PD-0332991 in selected cell types. For comparison purposes, combination of PD-0332991 and clinically-used gemcitabine/nab-paclitaxel[8] was found to significantly enhance apoptosis in RB-high TKCC-05 (compared with gemcitabine/nab-paclitaxel; supplementary figure S5C), although gemcitabine/PD-0332991 effects appeared more robust (across early/late timepoints, figure 1G).

To examine quiescence-associated alterations in cell cycle dynamics, we used an established flow cytometric methodology[26] to analyze FUCCI and quantify G_0 vs G_1 accumulation post-PD-0332991-based treatments (figure 1I). Both PD-0332991 and gemcitabine/PD-0332991 significantly increased the mKO2++ G_0 quiescent fraction,[26] compared with gemcitabine or vehicle specifically in the RB-high setting (figure 1J,K; supplementary figure S6). Cell cycle analysis of drug-treated apoptotic cells revealed most significant increases in the G_0 fraction post-PD-0332991-based therapy (supplementary figure S6E). Collectively, these findings provide evidence that activated apoptosis and G_0 quiescence are key mechanisms behind the observed synergy between gemcitabine and CDK4/6i in 2D.

CDK4/6 Inhibition Modulates the Invasiveness of RB-high PDA cells and ECM organization

A single study reported that following incubation with a high PD-0332991 concentration (5μM), selected commercial PDA lines displayed increased migratory capacity.[27] Because both 3D topology and mechanical cues provided by the stroma can shape and drive invasive tumor behavior,[28] we examined the effect of CDK4/6 inhibition on the invasive potential of RB-high and RB-negative PDA cells using an established three-dimensional organotypic model of invasion[6 29] (figure 2A). In 3D, PD-0332991 or gemcitabine individually significantly impaired invasion of RB-high TKCC-05 cells, with PD-032291 treatment being more effective (figure 2B, *left*, *middle*). Moreover, gemcitabine/PD-0332991 combination was markedly superior to each monotherapy (figure 2B, C). PD-0332991 did not affect the invasive capacity of RB-negative KPC cells in 3D (figure 2D). Further, the observed inhibitory effects on RB-high TKCC-05 invasion were accompanied by decreased proliferation and increased apoptosis in PD-0332991 and gemcitabine/PD-0332991-treated matrices (figure 2F-G, supplementary figure S7A-B). In contrast, PD-0332991 treatment slightly increased proliferation of invaded KPC cells, not affecting apoptosis (supplementary figure S7C-D). In 2D, gemcitabine/PD-0332991 reduced migratory capacity of RB-high TKCC-05 cells (supplementary figure S8), although PD-0332991-mediated effects were more pronounced in 3D, highlighting potential intricacies of CDK4/6-targeting of tumor cells within a complex microenvironment.

Since ECM deposition, fibrosis and signaling processes play a major role in regulating phenotype of pancreatic tumor cells and therapeutic response[6 30] we investigated the effect of CDK4/6i on ECM integrity using primary fibroblast-driven contraction assays[31], as recently achieved by our team (figure 2H).[32] PD-0332991 significantly impaired the ability of fibroblasts to contract (figure 2I) and remodel fibrillar collagen, as shown by second harmonic generation (SHG) imaging (figure 2J-

K; supplementary video S1), and bright-field/ polarized light microscopy of picrosirius red staining (figure 2L-0), indicating a significantly disorganized ECM network in PD-0332991-treated matrices. Impairment of matrix contraction was independent of changes in fibroblast proliferation (in 2D and 3D; supplementary figure S9). As these experiments revealed a significant anti-invasive, anti-proliferative and ECM-modulatory activity of PD-0332991 in complex 3D settings, we therefore sought to assess whether PD-0332991 and combinations affect PDA progression and drug response *in vivo.*

CDK4/6i Mono- and Combination Therapy Significantly Improve Survival of Mice Engrafted with RB-High Patient-Derived Pancreatic Tumors

Therapeutic responsiveness in our early-passage patient-derived xenografts (PDXs) was determined by measuring tumor growth, with experimental design (figure 3A, supplementary figure S10A) enabling assessment of initial therapeutic responsiveness, and longitudinal analysis, comparing intrinsically resistant tumors to those that acquire resistance over time, as previously described.[5 33 34] Strikingly, subtype-specific *in vivo* efficacy was observed, with all three RB-high PDXs examined showing significant long-term inhibition of tumor growth and improvement in overall survival following PD-0332991 monotherapy or gemcitabine/PD-0332991 treatment, compared with standard-of-care (gemcitabine and gemcitabine/nab-Paclitaxel; figure 3B-D, supplementary table S4A-C). Since gemcitabine/nab-Paclitaxel was associated with cumulative intestinal toxicity when administered over 4-5 treatment cycles, efficacy of targeted therapies was compared to gemcitabine only in the gemcitabine-sensitive TKCC-PDX-26. In addition to improving survival, we observed significantly improved relapse-free survival (defined in supplementary figure S10) following gemcitabine/PD-0332991, compared with gemcitabine

(supplementary figure S10B). In contrast, RB-negative TKCC-PDX-27, RB-low TKCC-PDX-16 and RB-negative KPC orthografts were resistant to PD-0332991-based therapy (figure 3E-G, supplementary table S5A-C). “On-target” modulation was confirmed by measuring inhibition of pRB and proliferation (Ki-67; supplementary figure S11A,B) in PD-0332991-treated RB-high PDX-05.

Analysis of PD-0332991 and gemcitabine/PD-0332991-treated RB-high tumor remnants revealed significant, prolonged *in vivo* inhibition of proliferation and increased apoptosis (figure 3H-K), also associated with decreased α-smooth muscle actin expression (figure 3L-M; supplementary figure S11C), prototypical marker of activated pancreatic stellate cells (PSCs), which drive the extensive fibrosis typically observed in PDA.[35] [36] In PD-0332991-resistant tumors, only gemcitabine/nab-Paclitaxel treatment showed any significant modulatory effects (supplementary figure S11D-F). In agreement with IHC analyses, the significant tumor regression observed in RB-high and *CDK6*-amplified PDXs post-treatment (30-day timepoint; supplementary figure S11G), further supports the idea that in addition to its cytostatic activity, PD-0332991 may exert cytotoxic effects on specific PDA subtypes *in vivo*.

PD-0332991-Based Therapeutic Interventions Inhibit Spread in the Liver While Sensitizing RB-high Tumor Cells to Shear Stress and Reducing Cell Attachment

Next, we performed intrasplenic injections of RB-high TKCC-05-FUCCI cells in parallel with systemic PD-0332991 administration as a way of examining efficacy of PD-0332991-based therapies in limiting pancreatic cancer spread to distant sites (figure 4A). Pathology analyses on serial sections of liver metastases (figure 4B,C) confirmed that mice treated with PD-0332991 and gemcitabine/PD-0332991 showed

a marked reduction in metastatic spread compared to gemcitabine/nab-Paclitaxel. FUCCI analyses of the same liver tissues further confirmed *in vivo* PD-0332991 activity and ability to effectively inhibit CDK4/6 in liver metastases (figure 4D,E).

To further understand the observed PD-0332991-mediated reduction of liver colonization, we examined viability (apoptosis) and cell attachment of RB-high and for comparison, RB-negative PDA cells after exposure to controlled shear stress (100µL/sec, maximum force of 1950 dyn/cm^2, figure 4F)[6 37], which CTCs are exposed to *in vivo*. PD-0332991 significantly induced post-stress cellular apoptosis and decreased cell attachment onto a collagen matrix, specifically in RB-high tumor cells (figure 4G-I, J-K). Collectively, these experiments suggest a direct role of CDK4/6 targeting in sensitizing CTCs already exposed to shear stress as a potential mechanism in which PD-0332991 may modulate metastasis in PDA.

PD-0332991-Based Therapies Significantly Improve Survival and Delay Metastasis in Metastatic RB-High PDA

To examine the effect of CDK4/6i on PDA tumor progression and metastasis, mice were orthotopically injected with luciferase-TKCC-05 tumors, imaged 1 week post-injection (supplementary figure S12A), randomized and treated with standard chemotherapies, PD-0332991, and PD-0332991-based combinations, until ethical endpoint (figure 5, *top*).

Critically, PD-0332991-based regimens were significantly more effective than standard therapies (figure 5A, *bottom*, supplementary table S6) in RB-high metastatic PDA, with gemcitabine/PD-0332991 proving the best therapeutic approach (Median survival= 117 days, p=0.0001; vs gemcitabine/nab-Paclitaxel Median survival= 69 days). In addition, metastasis-free survival, monitored by IVIS imaging

(supplementary figure S12B-C), was significantly increased by PD-0332991-based treatments (supplementary figure S13A, supplementary table S7). Given *in vitro* efficacy was observed when PD-0332991 was combined with gemcitabine/nab-Paclitaxel (supplementary figure S5), we also examined this combination *in vivo*. While treatments were generally well tolerated in experimental animals, the two triple combinations examined using gemcitabine/nab-Paclitaxel and PD-0332991 were associated with some toxicity, namely constipation, which was treated with paraffin oil and controlled by adjusting PD-0332991 dosage. Both regimens, involving concomitant PD-0332991 administration (concomitant), or aiming to assess the potential of CDK4/6i as maintenance therapy in between chemotherapy cycles (maintenance), demonstrated a significant therapeutic benefit over gemcitabine/nab-Paclitaxel (figure 5A, *bottom right*, supplementary table S6-7), but were not superior to gemcitabine/PD-0332991.

Following initial treatment with gemcitabine/nab-Paclitaxel, a short-term response was followed by progression, measured as increased bioluminescence signal (supplementary figure S12C). To examine the therapeutic potential of gemcitabine/PD-0332991 in slowing PDA progression in advanced disease settings, separate cohorts of relapsed animals were subsequently switched to gemcitabine/PD-0332991 or as control, clinically used 2nd line therapy, capecitabine[38] [39], with a superior therapeutic benefit measured with gemcitabine/PD-0332991 (figure 5B, supplementary table S6-7). In concordance, analyses of orthotopic FUCCI-TKCC-05 tumors collected 50 days post-treatment, revealed marked quiescence at the primary site (pancreas tumor), regardless of proximity to vessels (figure 5C-E, supplementary figure S13B-C), and no liver metastases in animals treated with PD-0332991 or gemcitabine/PD-0332991 (figure 5C,F). SHG imaging and polarized light

microscopy of picrosirius red-stained TKCC-05-FUCCI tumors confirmed that PD-0332991-based therapy reduces fibrillar collagen organization (figure 5G-H; supplementary figure S14A), leads to increased apoptosis and decreased expression of α-smooth muscle actin *in vivo* (supplementary figure S14B-C).

These data indicate that CDK4/6 inhibition significantly delays pancreatic tumor progression by directly targeting tumor cells (G_0 quiescence, apoptosis) and critical components of the microenvironment that have been shown to regulate chemoresistance (i.e. decreased stromal activation, reduced fibrillar collagen organization). As robust efficacy was observed in multiple, independent models of RB-high PDA, RB-based stratification could potentially facilitate a more tailored treatment approach for CDK4-targeting therapy in pancreatic cancer.

Nuclear RB is Prevalent in Primary Operable and Metastatic Human PDA and Has Prognostic Value

Next, we immunohistochemically examined the expression of RB in human PDA and whether its disruption has prognostic significance (figure 6A). High RB expression was detected in 64.5% of primary tumor specimens from the APGI/ICGC cohort[1] (*n*=200) and correlated with significantly improved survival (figure 6B-C, supplementary table S8) and lower tumor grade (supplementary table S9). Multivariate analysis using a Cox proportional hazards model demonstrated RB loss as an independent poor prognostic factor for disease-specific survival (hazard ratio 1.552, p=0.0148, table 1). In contrast, p16 expression, examined for comparison purposes, was not prognostic (supplementary figure S15A-D). Deregulation of RB signaling has been linked with improved chemo-responsiveness in breast cancer,[40] however when correlated, RB expression did not specifically associate with survival

following adjuvant gemcitabine (supplementary figure S15E-F). As expected, RB and p16 levels strongly correlated in the PDX (*n*=45) and patient tumors from which they were derived (p<0.001, supplementary table S10).

The potential prognostic value of RB was subsequently validated in an independent patient NSWPCN cohort[20] (*n*=314), where similar relationships between RB expression and survival were apparent in univariate (figure 6D-E, supplementary table S8) and multivariate analyses (hazard ratio 1.364, p=0.02, table 1). As most patients present with advanced stage PDA, we also assessed RB status in metastatic disease (*n*=54; supplementary table S11-S12). RB protein was highly expressed in 67% of metastatic specimens. Concordance in RB expression between matched primary and metastatic tumors of PDA, available for 12 of the 54 metastatic samples, was observed in 11 cases (91.7%; Cohen's kappa score 0.75; figure 6F-G) indicating the strength of the agreement as "good".

Collectively, these data demonstrate that a significant proportion of primary operable and metastatic PDA express high levels of the prognostically-relevant RB. This druggable, constitutively active pathway may represent an attractive therapeutic target, with immunohistochemical analysis of RB as a potentially simple prognostic and predictive biomarker to guide this therapeutic approach.

Table 1. Multivariate analysis of RB and key factors associated with disease-specific survival (DSS) in independent clinical cohorts of resected PDA.

	APGI cohort (*n*=200)			NSWPCN cohort (*n*=314)		
Variable	**HR**	**CI 95%**	**P value**	**HR**	**CI 95%**	**P value**
Gender						
Female				1.15	0.899-1.471	0.2656
Male				1		
R status						
Clear	0.712	0.482-1.052	0.0882	0.635	0.492-0.821	**0.0005**
Involved	1			1		
Differentiation						
Well/Moderate	0.384	0.046-3.224	**0.0022**	0.802	0.607-1.060	0.1216
Poor/ Undifferentiated	1			1		
Perineural invasion						
Absent	0.818	0.484-1.382	0.452	0.917	0.692-1.216	0.5467
Present	1			1		
Tumor size						
<20mm	0.663	0.315-1.396	0.2795	0.563	0.413-0.769	**0.0003**
>=20mm	1			1		
Lymphovascular invasion						
Absent	0.729	0.475-1.120	0.1496	0.864	0.669-1.117	0.2642
Present	1			1		
Lymph node involvement						
Absent	0.736	0.446-1.213	0.2287	0.735	0.564-0.956	**0.0218**
Present	1			1		
AJCC stage[32]						
Stage I/II	0.731	0.335-1.598	0.4325	0.425	0.228-0.790	**0.0068**
Stage III/IV	1			1		
RB status						
RB 0 or 1+	1.552	1.090-2.210	**0.0148**	1.364	1.048-1.776	**0.0209**
RB 2+	1			1		

* HR denotes hazard ratio, CI confidence interval.

DISCUSSION

Despite significant recent efforts into developing novel treatment combinations,[41] chemotherapy remains the standard-of-care for most patients with advanced pancreatic cancer, despite only modestly improving survival.[8] With rapid implementation in the clinical management of specific breast cancers, CDK4/6i are increasingly being tested in other solid tumors.[42 43] Here, we examined whether CDK4 pathway inhibition in combination with chemotherapy, represented a viable therapeutic approach for pancreatic tumors characterized by G_1/S checkpoint aberrations, frequent in the molecular landscape of PDA.[1] We demonstrate potent efficacy of single agent and combination CDK4/6i therapy in subtypes of PDA characterized by high RB expression, significantly improving long-term survival while delaying the development of metastasis in robust *in vivo* models of PDA. We also reveal that the potent efficacy of CDK4/6i mono- and combination therapy occurs via a complex mechanism involving deregulation of tumor cell signaling and disruption of the surrounding ECM that collectively drive cancer cell proliferation, invasion, and metastasis,[6 30 44] while revealing a new role of CDK4/6 inhibition in governing tolerance to shear stress, an often overlooked area of pre-metastatic niche formation for CTCs.[45 46]

A major area of active investigation is the identification of biomarkers of therapeutic response to CDK4 inhibition. In preclinical models of melanoma and glioblastoma, homozygous loss, methylation, or mutation of *CDKN2A* gene were shown to associate with sensitivity to CDK4/6i,[47 48] although in the clinic, CDK4/6i sensitivity may not be strictly defined by p16 status.[49] Here we show that RB expression, but

not G_1/S checkpoint mutations or p16 levels, may present a robust stratifying biomarker for PD-0332991-based therapy in advanced preclinical models of PDA.

PD-0332991 has traditionally been thought to exert its anti-tumor effects by promoting cytostasis, also supported by limited data in PDA, whereby using 7-day assessment of proliferation as a read-out of PD-0332991 activity, early efficacy has been measured in almost all PDA explants examined.[18] Deeper exploration of the long-term responsiveness to PD-0332991 and combination therapy, directly compared with standard-of-care treatments, in this study, highlights the need for a personalized approach in the treatment of pancreatic cancer, where RB-high PDA tumors respond long-term to PD-0332991-based therapy *in vivo* and RB-low/negative tumors do not. Moreover, building on recent studies in other cancers, which suggest a more complex mechanism of action for CDK4/6i, including inhibition of EMT signaling in breast cancer metastasis[50] and improved anti-tumor immunity,[51] our study provides additional new evidence that PD-0332991 displays multifaceted effects on tumor cells (quiescence, apoptosis), alters ECM organization and reduces tolerance to shear stress (figure 4), thereby having a global effect in this aggressive disease, not examined previously.

Using a combination of 2D, 3D *in vitro* and *in vivo* models we specifically show that PD-0332991 significantly induces apoptosis in RB-high pancreatic tumor settings, and also enhances the apoptotic effect of chemotherapeutic gemcitabine, a well-tolerated and clinically-used agent in PDA (figure 1-3). Monitoring the onset of liver metastasis *in vivo* revealed that PD-0332991 mono- and combination therapy significantly impaired liver colonization in the RB-high setting (figure 4A-E), delaying disease progression in a metastatic PDA model (figure 5). Of note, CDK4/6i may potentially be a beneficial 2nd line therapy, following progression on gemcitabine/nab-

Paclitaxel in RB-high PDA, as our *in vivo* findings suggest (figure 5B). Given the high rate of chemotherapeutic resistance in advanced PDA patients treated with these chemotherapies and their subsequent extremely poor outcome, pending further pre-clinical study, CDK4/6i-based approaches may potentially be a viable 2nd line treatment for specific subtypes of advanced PDA.

CDK4/6 inhibition modulated ECM organization *in vitro* and *in vivo* (figure 2, 5), with *in vivo* responses to PD-0332991-based therapy associated with decreased expression of α-smooth muscle actin, marker of activated PSCs and stromal activation. As our *in vitro* findings suggest that the effects on ECM are independent of the anti-proliferative activity of PD-0332991, it is plausible to hypothesize that changes in ECM mechanics induced by PD-0332991 may directly disrupt PSC activation, the subsequent tumor cell-PSC crosstalk and ultimately further improve therapeutic sensitivity. Indeed, recent work has shown that matrix stiffness and organization can directly regulate differentiation and migration of PSCs.[52]

PD-0332991 and gemcitabine strongly synergized irrespective of p16 or p53 status (for example whether pancreatic tumor harbored an inactivating *TP53* mutation (C124*; PDX-26), mutation contributing to partial rescue (V173M; PDX-03) or higher than wild-type p53 activity (G245S; PDX-05).[53] *CDK*4/*CDK*6 amplification or overexpression has been associated with *in vitro* CDK4/6i resistance,[47] although *CDK*4-amplified liposarcomas are sensitive to PD-0332991.[54] Interestingly, the *CDK*6-amplified PDX-26 and matched PDCL responded to PD-0332991-based treatment, suggesting that in PDA *CDK*6 amplification in the context of functional RB does not preclude effective CDK4 pathway inhibition. Although CDK6 is strongly functionally linked to CDK4, this enzyme may exert other kinase-independent

functions in regulation of angiogenesis and/or cell differentiation,[55] representing a potentially separate thus far unexamined role for CDK6 inhibition in PDA therapy.

Several smaller studies have investigated the prognostic role of RB in PDA, with inconsistent findings.[56] Here, RB protein was highly expressed in a significant proportion of PDA (65%, APGI/ICGC; 43%, NSWPCN; 67%, metastatic cohort), suggesting that this could be a viable therapeutic target for tailored CDK4/6i-based treatments that act on this signaling network. Moreover, the observed concordance in RB levels in the small set of available matched primary and metastatic tissue, lends hope that metastases may still be co-targeted with this type of therapy. Loss of RB protein was associated with poor patient outcome, with RB an independent prognostic factor for disease-specific survival in two sizeable independent PDA cohorts (table 1). RB immunohistochemistry was a clean nuclear stain without considerable background. In our hands, it appeared comparable to ER staining in terms of interpretation of intensity within processed material. Pending further validation, use of a tissue-based assay for RB expression could be adapted for clinical application in diagnostics to, combined with other markers, help identify those with poorest prognoses and also potentially identify a cohort of patients to trial CDK4/6i.

In conclusion, we provide pre-clinical proof-of-concept for the efficacy of a personalized treatment strategy using CDK4/6i to treat RB-high PDA. We reveal key mechanisms whereby CDK4-targeting therapy may regulate multiple cellular processes and environmental cues within the primary tumor, secondary site and during CTC transit, which collectively govern pancreatic cancer progression. We hope that, with two non-biomarker driven phase I/II trials of PD-0332991 in pancreatic cancer underway (NCT02501902, NCT03065062), these findings may

have complementary and potentially significant therapeutic implications for the personalized treatment of PDA in future.

ACKNOWLEDGEMENTS: The authors would like to thank consumer representatives Prof Ros Pesman, Mr Benjamin Bravery and Ms Jan Mumford for their involvement in this project and a critical review of the manuscript. Dr Chou would also like to acknowledge Associate Professor Adrienne Morey for mentorship during PhD studies.

AUTHOR CONTRIBUTIONS: Study concept and design (MP, AJG, AC, SJC, PT); data acquisition (AC, DF, AMN, VTC, DW, AM, AS, RS, AD, KJM, JT); analysis and data interpretation (AC, DF, DW, AM, TRC, TJM, JT, CV, KJM, AB, OJS, JM); drafting of manuscript (AC, DF, MP); critical review and edit of manuscript (AJG, PT, AJ, SJC, JS, NW, SMG, LAC, AB, TRC, AVB, TJM, OJS, JM); patient cohort data (APGI, AJ, AVB, JS, AJG, JT, SMG); statistics (AC, MC, MP, DKC); obtained funding (MP, AJG, AC, SJC, PT, JS, AMN, AB, NW); study supervision (MP, AJG).

CONFLICTS OF INTEREST: The authors have declared that no conflict of interest exists.

GRANT SUPPORT: This work was supported by the National Health and Medical Research Council of Australia (NHMRC) Project Grants 1081312 and 1105640, Cancer Australia Project Grants 1060522 and 1100722 with fellowship support from Cancer Institute NSW 13/CDF/1-01, 2017/CDF002 and NHMRC 1112113, scholarship support from NHMRC 1039812 and Sydney Catalyst and philanthropic support from the Avner Pancreatic Cancer Foundation, The Philip Hemstritch Fellowship in Pancreatic Cancer; Len Ainsworth Pancreatic Cancer Fellowship, Estate of the late RT Hall Cancer Gene Discovery and Validation Program and Norman Green Support Grant.

REFERENCES

1. Bailey P, Chang DK, Nones K, et al. Genomic analyses identify molecular subtypes of pancreatic cancer. *Nature* 2016;531(7592):47-52.
2. Jones S, Zhang X, Parsons DW, et al. Core signaling pathways in human pancreatic cancers revealed by global genomic analyses. *Science* 2008;321(5897):1801-6.
3. Collisson EA, Sadanandam A, Olson P, et al. Subtypes of pancreatic ductal adenocarcinoma and their differing responses to therapy. *Nat Med* 2011;17(4):500-3.
4. Integrated Genomic Characterization of Pancreatic Ductal Adenocarcinoma. *Cancer Cell* 2017;32(2):185-203.e13.
5. Waddell N, Pajic M, Patch AM, et al. Whole genomes redefine the mutational landscape of pancreatic cancer. *Nature* 2015;518(7540):495-501.
6. Vennin C, Chin VT, Warren SC, et al. Transient tissue priming via ROCK inhibition uncouples pancreatic cancer progression, sensitivity to chemotherapy, and metastasis. *Sci Transl Med* 2017;9(384)
7. Burris HA, 3rd, Moore MJ, Andersen J, et al. Improvements in survival and clinical benefit with gemcitabine as first-line therapy for patients with advanced pancreas cancer: a randomized trial. *J Clin Oncol* 1997;15(6):2403-13.
8. Von Hoff DD, Ervin T, Arena FP, et al. Increased Survival in Pancreatic Cancer with nab-Paclitaxel plus Gemcitabine. *N Engl J Med* 2013;369(18):1691-703.
9. Conroy T, Desseigne F, Ychou M, et al. FOLFIRINOX versus gemcitabine for metastatic pancreatic cancer. *N Engl J Med* 2011;364(19):1817-25.
10. O'Hayer KM, Brody JR. Personalized therapy for pancreatic cancer: Do we need better targets, arrows, or both? *Discovery medicine* 2016;21(114):117-23.

11. Schutte M, Hruban RH, Geradts J, et al. Abrogation of the Rb/p16 tumor-suppressive pathway in virtually all pancreatic carcinomas. *Cancer Res* 1997;57(15):3126-30.
12. O'Leary B, Finn RS, Turner NC. Treating cancer with selective CDK4/6 inhibitors. *Nat Rev Clin Oncol* 2016;13(7):417-30.
13. Sheppard KE, McArthur GA. The cell-cycle regulator CDK4: an emerging therapeutic target in melanoma. *Clin Cancer Res* 2013;19(19):5320-8.
14. Cristofanilli M, Turner NC, Bondarenko I, et al. Fulvestrant plus palbociclib versus fulvestrant plus placebo for treatment of hormone-receptor-positive, HER2-negative metastatic breast cancer that progressed on previous endocrine therapy (PALOMA-3): final analysis of the multicentre, double-blind, phase 3 randomised controlled trial. *Lancet Oncol* 2016;17(4):425-39.
15. Finn RS, Crown JP, Lang I, et al. The cyclin-dependent kinase 4/6 inhibitor palbociclib in combination with letrozole versus letrozole alone as first-line treatment of oestrogen receptor-positive, HER2-negative, advanced breast cancer (PALOMA-1/TRIO-18): a randomised phase 2 study. *Lancet Oncol* 2015;16(1):25-35.
16. Sledge GW, Jr., Toi M, Neven P, et al. MONARCH 2: Abemaciclib in Combination With Fulvestrant in Women With HR+/HER2- Advanced Breast Cancer Who Had Progressed While Receiving Endocrine Therapy. *J Clin Oncol* 2017:Jco2017737585.
17. Wander SA, Mayer EL, Burstein HJ. Blocking the Cycle: Cyclin-Dependent Kinase 4/6 Inhibitors in Metastatic, Hormone Receptor-Positive Breast Cancer. *J Clin Oncol* 2017:Jco2017739482.

18. Witkiewicz AK, Borja NA, Franco J, et al. Selective impact of CDK4/6 suppression on patient-derived models of pancreatic cancer. *Oncotarget* 2015;6(18):15788-801.
19. Alvarez R, Musteanu M, Garcia-Garcia E, et al. Stromal disrupting effects of nab-paclitaxel in pancreatic cancer. *Br J Cancer* 2013;109(4):926-33.
20. Chang DK, Johns AL, Merrett ND, et al. Margin clearance and outcome in resected pancreatic cancer. *J Clin Oncol* 2009;27(17):2855-62.
21. Hingorani SR, Wang L, Multani AS, et al. Trp53R172H and KrasG12D cooperate to promote chromosomal instability and widely metastatic pancreatic ductal adenocarcinoma in mice. *Cancer Cell* 2005;7(5):469-83.
22. Morran DC, Wu J, Jamieson NB, et al. Targeting mTOR dependency in pancreatic cancer. *Gut* 2014;63(9):1481-9.
23. Chou TC. Drug combination studies and their synergy quantification using the Chou-Talalay method. *Cancer Res* 2010;70(2):440-6.
24. Sakaue-Sawano A, Kurokawa H, Morimura T, et al. Visualizing spatiotemporal dynamics of multicellular cell-cycle progression. *Cell* 2008;132(3):487-98.
25. Hill R, Rabb M, Madureira PA, et al. Gemcitabine-mediated tumour regression and p53-dependent gene expression: implications for colon and pancreatic cancer therapy. *Cell death & disease* 2013;4:e791.
26. Tomura M, Sakaue-Sawano A, Mori Y, et al. Contrasting quiescent G0 phase with mitotic cell cycling in the mouse immune system. *PLoS One* 2013;8(9):e73801.
27. Liu F, Korc M. Cdk4/6 inhibition induces epithelial-mesenchymal transition and enhances invasiveness in pancreatic cancer cells. *Mol Cancer Ther* 2012;11(10):2138-48.

28. Rath N, Olson MF. Regulation of pancreatic cancer aggressiveness by stromal stiffening. *Nat Med* 2016;22(5):462-3.

29. Timpson P, McGhee EJ, Morton JP, et al. Spatial regulation of RhoA activity during pancreatic cancer cell invasion driven by mutant p53. *Cancer Res* 2011;71(3):747-57.

30. Laklai H, Miroshnikova YA, Pickup MW, et al. Genotype tunes pancreatic ductal adenocarcinoma tissue tension to induce matricellular fibrosis and tumor progression. *Nat Med* 2016;22(5):497-505.

31. Kosako H, Yoshida T, Matsumura F, et al. Rho-kinase/ROCK is involved in cytokinesis through the phosphorylation of myosin light chain and not ezrin/radixin/moesin proteins at the cleavage furrow. *Oncogene* 2000;19(52):6059-64.

32. Mayorca-Guiliani AE, Madsen CD, Cox TR, et al. ISDoT: in situ decellularization of tissues for high-resolution imaging and proteomic analysis of native extracellular matrix. *Nat Med* 2017;23(7):890-98.

33. Pajic M, Iyer JK, Kersbergen A, et al. Moderate increase in Mdr1a/1b expression causes in vivo resistance to doxorubicin in a mouse model for hereditary breast cancer. *Cancer Res* 2009;69(16):6396-404.

34. Pajic M, Blatter S, Guyader C, et al. Selected alkylating agents can overcome drug tolerance of G0-like tumor cells and eradicate BRCA1-deficient mammary tumors in mice. *Clinical cancer research* 2017

35. Apte MV, Park S, Phillips PA, et al. Desmoplastic reaction in pancreatic cancer: role of pancreatic stellate cells. *Pancreas* 2004;29(3):179-87.

36. Apte MV, Wilson JS, Lugea A, et al. A starring role for stellate cells in the pancreatic cancer microenvironment. *Gastroenterology* 2013;144(6):1210-9.

37. Barnes JM, Nauseef JT, Henry MD. Resistance to Fluid Shear Stress Is a Conserved Biophysical Property of Malignant Cells. *PLoS One* 2012;7(12)

38. Heinemann V, Vehling-Kaiser U, Waldschmidt D, et al. Gemcitabine plus erlotinib followed by capecitabine versus capecitabine plus erlotinib followed by gemcitabine in advanced pancreatic cancer: final results of a randomised phase 3 trial of the 'Arbeitsgemeinschaft Internistische Onkologie' (AIO-PK0104). *Gut* 2013;62(5):751-9.

39. Network NCC. NCCN Clinical Practice Guidelines in Oncology Pancreatic Adenocarcinoma (Version 2.2017) 2017 [Available from: https://www.nccn.org/professionals/physician_gls/pdf/pancreatic.pdf accessed August 16, 2017.

40. Witkiewicz AK, Ertel A, McFalls J, et al. RB-pathway Disruption is Associated with Improved Response to Neoadjuvant Chemotherapy in Breast Cancer. *Clin Cancer Res* 2012;18(18):5110-22.

41. Dizon DS, Krilov L, Cohen E, et al. Clinical Cancer Advances 2016: Annual Report on Progress Against Cancer From the American Society of Clinical Oncology. *J Clin Oncol* 2016;34(9):987-1011.

42. Chiron D, Di Liberto M, Martin P, et al. Cell-cycle reprogramming for PI3K inhibition overrides a relapse-specific C481S BTK mutation revealed by longitudinal functional genomics in mantle cell lymphoma. *Cancer discovery* 2014;4(9):1022-35.

43. Gelbert LM, Cai S, Lin X, et al. Preclinical characterization of the CDK4/6 inhibitor LY2835219: in-vivo cell cycle-dependent/independent anti-tumor activities alone/in combination with gemcitabine. *Invest New Drugs* 2014;32(5):825-37.

44. Kai F, Laklai H, Weaver VM. Force Matters: Biomechanical Regulation of Cell Invasion and Migration in Disease. *Trends in cell biology* 2016;26(7):486-97.

45. Ritsma L, Steller EJ, Beerling E, et al. Intravital microscopy through an abdominal imaging window reveals a pre-micrometastasis stage during liver metastasis. *Sci Transl Med* 2012;4(158):158ra45.

46. Steeg PS. Targeting metastasis. *Nat Rev Cancer* 2016;16(4):201-18.

47. Cen L, Carlson BL, Schroeder MA, et al. p16-Cdk4-Rb axis controls sensitivity to a cyclin-dependent kinase inhibitor PD0332991 in glioblastoma xenograft cells. *Neuro-oncology* 2012;14(7):870-81.

48. Konecny GE, Winterhoff B, Kolarova T, et al. Expression of p16 and retinoblastoma determines response to CDK4/6 inhibition in ovarian cancer. *Clin Cancer Res* 2011;17(6):1591-602.

49. Michel L, Ley J, Wildes TM, et al. Phase I trial of palbociclib, a selective cyclin dependent kinase 4/6 inhibitor, in combination with cetuximab in patients with recurrent/metastatic head and neck squamous cell carcinoma. *Oral oncology* 2016;58:41-8.

50. Liu T, Yu J, Deng M, et al. CDK4/6-dependent activation of DUB3 regulates cancer metastasis through SNAIL1. *Nature communications* 2017;8:13923.

51. Goel S, DeCristo MJ, Watt AC, et al. CDK4/6 inhibition triggers anti-tumour immunity. *Nature* 2017

52. Lachowski D, Cortes E, Pink D, et al. Substrate Rigidity Controls Activation and Durotaxis in Pancreatic Stellate Cells. *Scientific reports* 2017;7(1):2506.

53. Baroni TE, Wang T, Qian H, et al. A global suppressor motif for p53 cancer mutants. *Proc Natl Acad Sci U S A* 2004;101(14):4930-5.

54. Dickson MA, Schwartz GK, Keohan ML, et al. Progression-Free Survival Among Patients With Well-Differentiated or Dedifferentiated Liposarcoma Treated With CDK4 Inhibitor Palbociclib: A Phase 2 Clinical Trial. *JAMA oncology* 2016;2(7):937-40.

55. Kollmann K, Heller G, Schneckenleithner C, et al. A kinase-independent function of CDK6 links the cell cycle to tumor angiogenesis. *Cancer Cell* 2013;24(2):167-81.

56. Smith RA, Tang J, Tudur-Smith C, et al. Meta-analysis of immunohistochemical prognostic markers in resected pancreatic cancer. *Br J Cancer* 2011;104(9):1440-51.

FIGURE LEGENDS

Figure 1. PD-0332991 potentiates gemcitabine (GEM) lethality in stratified pancreatic cancer PDCLs, and leads to increased apoptosis and G_0 cell cycle quiescence. (A) Correlation of PD-0332991 sensitivity and expression of *(left)* RB or *(right)* pRB in 19 PDCLs (normalized to β-actin levels and to low-expressing TKCC-16; included on multiple gels to account for any inter-gel/transfer variability). For densitometry analysis of normalized protein expression and correlation summaries please refer to supplementary table S2 and 3. (B) Expression of pRB in RB-high (TKCC-03, TKCC-05, TKCC-26) and RB-negative (TKCC-27) PDCLs 24h post-PD-0332991 treatment (0.3μM or 1μM, respectively). (C) Western blot depicting negligible levels of pRB and RB proteins in pancreatic cancer cells isolated from the genetically-engineered Pdx1-Cre; KrasLSL.G12D/+; p53R172H/+ (KPC) model of pancreatic cancer. Combination index (CI) of the GEM/PD-0332991 combination when agents were combined at a fixed ratio derived from their respective IC_{50} values in (D) RB-high and (E) RB-low/negative PDCLs. CI values determined at various effective doses (EDs) were calculated using CompuSyn program. CI>1 indicates antagonism, CI<1 synergy and CI=1 additive.[23] Data presented as mean ± SEM; (*n*=4 independent experiments performed in triplicate). *Inset*: Heat maps showing viability and CI values of GEM/PD-0332991 combination in various ratios in candidate (D) RB-high (TKCC-03) and (E) RB-negative cells (TKCC-27; *n*=3 independent experiments performed in triplicate). (F) FUCCI-labelled TKCC-05 or TKCC-27 cells were treated with GEM (0.01μM for both), PD-0332991 (0.3μM or 1μM, respectively) or combination and at selected time-points (3-10 days) stained with Annexin-V-Cy5/DAPI and analyzed using flow cytometry. Total apoptosis

quantified across all examined timepoints and treatments for (G) RB-high TKCC-05 and (H) RB-negative TKCC-27 cells. (I) Representative TKCC-05-FUCCI cell cycle plots and gating strategy post-treatment (10 days) and control. Quantified cell cycle distribution across all examined treatments (10 days timepoint) in (J) RB-high and (K) RB-negative PDCLs. *Inset*: Illustration of FUCCI cell cycle oscillations. Data shown as mean ± SEM (n=4 independent experiments), with comparisons performed against relevant vehicle controls, unless specified.

Figure 2. CDK4/6i inhibition impairs the invasive potential of RB-high PDA cells and disrupts collagen matrix integrity. (A) Schematic representation of organotypic invasion assay with PDA cells. (B) Invasion of vehicle- and drug-treated eGFP-luciferase-labeled TKCC-05 cells through 3D organotypic matrices over 21 days, indicated by GFP immunohistochemistry. (C) Quantification of cell invasion (100µm-400µm). (D) Invasion of vehicle- and PD-0332991-treated KPC cells through 3D organotypic matrices over 14 days, indicated by multi-cytokeratin staining and (E) quantified. (F) Representative images of Ki67 staining as a marker of cell proliferation and quantification of the percentage TKCC-05 cells positive for Ki67 in organotypic matrices following therapeutic intervention with PD-0332991-based approaches. (G) Representative images of cleaved caspase-3 (CC3) staining as a marker of cell apoptosis and quantification of TKCC-05 cells positive for CC3 (ratio normalized to control) in organotypic matrices post-treatment. (H) Schematic of a contraction assay *(top),* representative images of telomerase-immortalized fibroblast (TIF)–collagen control matrices *(bottom)* and (I) quantification of matrix area ± PD-0332991 at endpoint (9 days). (J) Representative maximum intensity projections of SHG signal and (K) quantification of SHG signal intensity at peak in TIF-collagen matrices after 9

days of contraction ± PD-0332991. (L) Bright-field and polarized light imaging of picrosirius red–stained TIF-collagen matrices ± PD-0332991 and quantification of total collagen content measured as (M) the total signal intensity (bright-field) and (N) intensity of the signal acquired via polarized light. (O) Contribution and quantification of signal emitted from fibers with high, medium, and low birefringence normalized to total signal acquired via polarized imaging of picrosirius red–stained collagen matrices ± PD-0332991. Thick remodeled collagen fibers are highly birefringent (red-orange), whereas less remodeled fibers have a lower birefringence (green). Data for organotypic and collagen contraction studies is presented as mean ± SEM (*n*=3 independent experiments, performed in triplicate matrices per condition, per repeat). Significance was determined by One-way ANOVA, followed by Tukey post hoc multiple comparisons test, where *p<0.05, **p<0.01, ***p<0.001 and ****p<0.0001. Unless specifically indicated, significance is compared against vehicle.

Figure 3. *In vivo* tailored response of PDA models to PD-0332991 and rationally designed treatment combinations. (A) Preclinical testing pipeline in subcutaneous models. Treatment commenced when tumors reached 150mm3 (100%), where each mouse was randomized into outlined treatment groups: (a) gemcitabine 120mg/kg twice weekly intraperitoneally (IP) for 25 days, (b) PD-0332991 150mg/kg daily gavage for 21 days, (c) gemcitabine (120mg/kg) twice weekly IP and PD-0332991 (150mg/kg) daily gavage or (d) gemcitabine (70mg/kg) and nab-Paclitaxel (30mg/kg) twice weekly IP for 25 days. In the combination arm, PD-0332991 was administered from week 2 for 21 days, 24h post-chemotherapy. Treatment response was measured from initiation of therapy (at maximal tolerable dose), through to the time resistance developed (characterized by progressive tumor growth in the presence of

drug), and was based on our published work, with a 14-day minimal recovery time before additional treatment cycles. Details on treatment administration are further outlined in supplementary information 2. (B-D) Kaplan-Meier survival analyses of response to PD-0332991 and GEM/PD-0332991 in PDXs stratified based on RB status, presented as overall survival. (E-G) Overall survival of immunocompromised or syngeneic mice bearing the RB-negative/low TKCC-PDX-27, PDX-16 and subcutaneous KPC tumors, respectively, treated with CDK4/6i monotherapy and combination, compared with standard therapies for PDA. (H) Representative images of Ki-67 immunohistochemistry performed on PDX-03 and (I) analyzed for RB-high PDXs post-treatment (collected at endpoint). (J) Representative images of cleaved caspase 3 (CC3) staining, marker of apoptosis, in PDX-03 and (K) quantified for RB-high PDXs. (L) Representative images of α-smooth muscle actin (SMA) stromal expression post-therapy and (M) staining quantified for RB-high PDXs across all treatment groups (*n*=6 mice per treatment group). Data shown as mean ± SD. Significance was determined by One-way ANOVA, followed by Tukey post hoc multiple comparisons test, where *p<0.05, **p<0.01, ***p<0.001 and ****p<0.0001. Unless specifically indicated, significance is compared against vehicle.

Figure 4. CDK4/6 inhibition decreases cell colonization and improves chemotherapy response in metastatic sites and makes RB-high tumor cells more vulnerable to shear stress. (A) Schematic representation of intrasplenic injection of RB-high TKCC-05-FUCCI cells and associated treatment timeline. (B) Representative images and (C) quantification of liver micro- and total metastases normalized to liver surface area in hematoxylin and eosin (H&E) serial sections. Arrows point to metastases in the liver tissue. Data shown as mean ± SD (*n* = 4 mice per group and five serial sections

per organ (50μm step). (D) Representative pictures of metastases identified via imaging of FUCCI signal and (E) quantified cell cycle distribution in liver metastases from the TKCC-05-FUCCI intrasplenic model at the experimental end point. (F) Schematic of the fluid shear stress assay, adapted from [37]. (G) Representative TKCC-05-FUCCI apoptosis plots and (H) quantification of total, early and late apoptosis in TKCC-05 cells ± PD-0332991 (0.3μM) 24 hours following shear stress. P0 represents cells not subjected to shear stress; P5, cells subjected to five consecutive exposures to shear stress. (I) Quantification of cell attachment onto the collagen matrix, following shear stress of RB-high TKCC-05 cells ± PD-0332991 treatment, measured 24 hours post-seeding. Y-axis values (P5/P0 ratios) are values for cells subjected to five exposures to shear stress divided by values for cells not exposed to shear stress (J) Quantification of apoptosis in RB-negative TKCC-27 cells ± PD-0332991 (1μM) 24 hours following shear stress. (K) Quantification of cell attachment onto the collagen matrix, following shear stress of RB-negative TKCC-27 cells ± PD-0332991 treatment. Data shown as mean ± SEM (*n* = 3 biological repeats with two collagen-coated wells per condition). Significance was determined by One-way ANOVA, followed by Tukey post hoc multiple comparisons test, where *p<0.05, **p<0.01, ***p<0.001 and ****p<0.0001. Unless specifically indicated, significance is compared against vehicle.

Figure 5. CDK4/6i therapy induces *in vivo* quiescence at primary tumor site, impairs metastatic spread, and improves gemcitabine efficacy in a metastatic patient-derived RB-positive model of PDA. (A) Schematic illustrating *in vivo* testing in a metastatic patient-derived model *(top)*. Briefly, 15,000 luciferase-labeled PDCLs were injected into the pancreas of 6-8 week old Nod/Scid/IL-2Rγnull (NSG) mice. Mice were

randomized into treatment groups at one week post-injection, with two additional treatment arms included, involving triple combination of gemcitabine (70mg/kg), nab-Paclitaxel (30mg/kg) twice weekly IP administered either concomitantly with PD-0332991 (100mg/kg) gavage from week 2 on a 5-day “on”, 5-day “off” schedule for 20 days, or with PD-0332991 administered as maintenance therapy by daily gavage after completion of gemcitabine/nab-Paclitaxel treatment. Tumor burden was monitored weekly by bioluminescent imaging until ethical endpoint. Kaplan-Meier survival analyses of PD-0332991 monotherapy, in combination with gemcitabine *(*GEM; *left)* or triple combinations with GEM/nab-Paclitaxel *(right),* compared with GEM/nab-Paclitaxel. (B) Experimental set-up for *in vivo* second-line therapeutic testing in metastatic PDA *(top)*. *In vivo* efficacy of GEM/PD-0332991 combination following recurrence on GEM/nab-Paclitaxel *(bottom)*. (C) Representative images of pancreas tumors (*left*) and associated liver metastases (*right*) from orthotopic FUCCI-TKCC-05 tumors collected 50 days post-treatment with CDK4/6i-based treatment or standard therapy (gemcitabine/nab-Paclitaxel). Vehicle controls were collected prior to the 50 day time-point, as expected, due to a heavy tumor burden. Shown is representative nuclear staining (DAPI, *top*), FUCCI (mKO2-red, mAG-green, overlay-yellow, CD31-blue; *middle*) and H&E section (*bottom*). Quantified cell cycle distribution of (D) primary tumors and (E) liver metastases from examined treatment groups, with (F) no metastases detected in PD-0332991 and GEM/PD-0332991 treated animals. (G) Representative overlay of maximum intensity projections of SHG signal and FUCCI with quantification of SHG signal intensity at peak in orthotopic FUCCI-TKCC-05 tumors collected post-treatment (H) Representative polarized light images of tumor tissue and quantification of total birefringence signal (black) and contribution to signal emitted from collagen fibers with high (red), medium (yellow),

and low (green) birefringence acquired via polarized light imaging (*n*=4 animals per treatment group were used for analysis in D, E, G and H).

Figure 6. High RB expression is prevalent in human PDA and is of prognostic relevance in independent cohorts of the disease. Examples of (A) *(left)* RB-negative primary tumor (0); *(middle)* Weakly RB-positive tumor (1+) and *(right)* RB-high tumor (2+). Kaplan-Meier analyses of disease-specific survival based on RB immunohistochemistry in (B and C) the APGI/ICGC cohort and (D and E) the NSWPCN patient cohort. Survival analyses were performed comparing (B and D) all three RB groups and (C and E) RB-high (2+) versus RB-low in both sets. *P* values, log-rank. (F) Examples of *(left)* RB-high and *(right)* RB-low primary tumors and matched metastases. (G) The agreement of RB status between primary and metastatic tumors of PDA. The number of observed agreements is 11 (91.67% of the observation), with a kappa score 0.75 (SE of kappa 0.232, 95% confidence interval 0.296 to 1.000), indicating the strength of agreement is “good”.

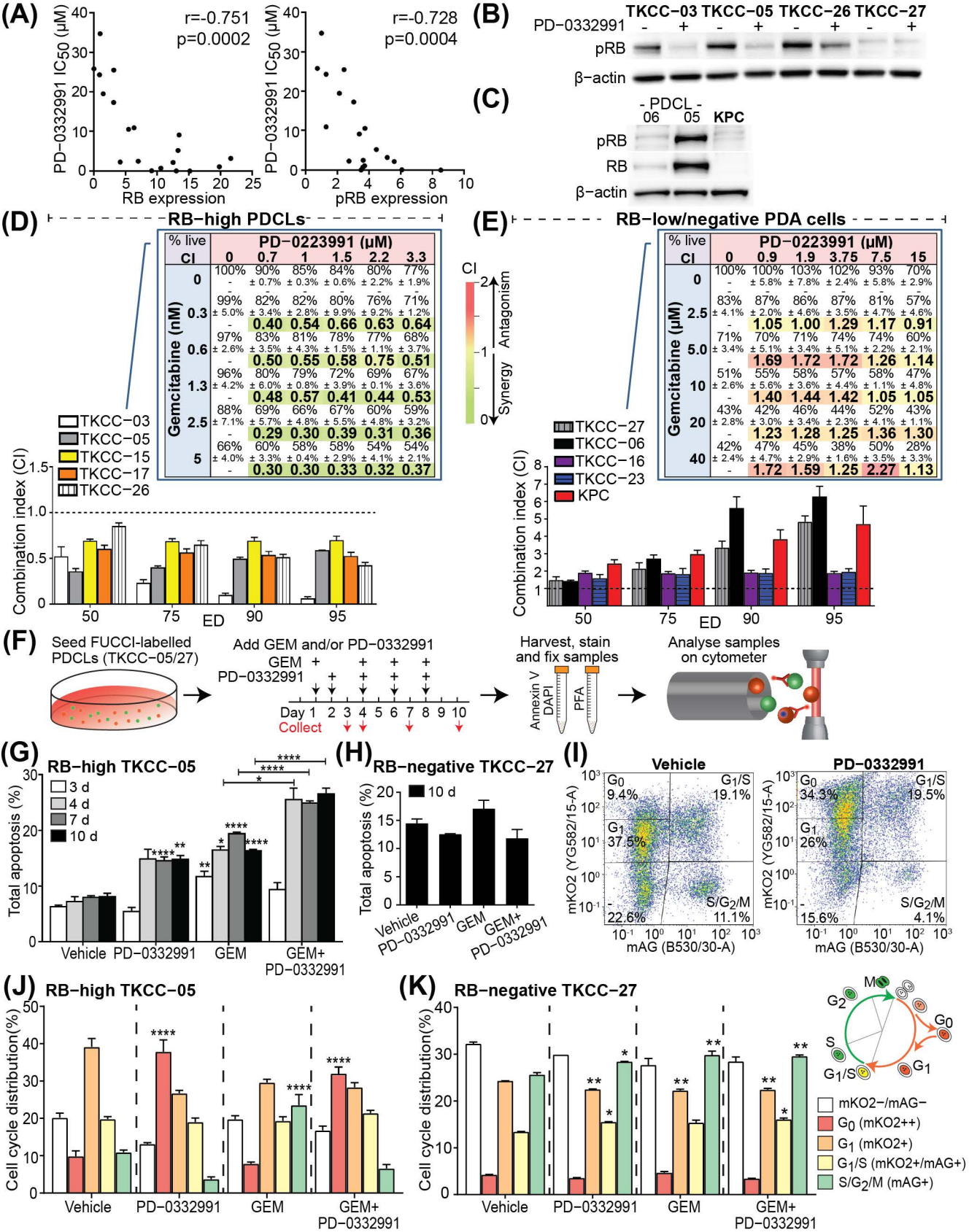
(A)
r=-0.751
p=0.0002
PD−0332991 IC50 (μM)
RB expression
r=-0.728
p=0.0004
pRB expression
(B)
TKCC−03 TKCC−05 TKCC−26 TKCC−27
PD−0332991
pRB
β−actin
(C)
- PDCL -
06 05 KPC
pRB
RB
β−actin
(D)
RB−high PDCLs
% live
CI
PD−0223991 (μM)
0 0.7 1 1.5 2.2 3.3
Gemcitabine (nM)
0 100% 90% 85% 84% 80% 77%
0.3 99% 82% 82% 80% 76% 71%
0.40 0.54 0.66 0.63 0.64
0.6 97% 83% 81% 78% 77% 68%
0.50 0.55 0.58 0.75 0.51
1.3 96% 80% 79% 72% 69% 67%
0.48 0.57 0.41 0.44 0.53
2.5 88% 69% 66% 67% 60% 59%
0.29 0.30 0.39 0.31 0.36
5 66% 60% 58% 58% 54% 54%
0.30 0.30 0.33 0.32 0.37
CI
Antagonism
Synergy
TKCC−03
TKCC−05
TKCC−15
TKCC−17
TKCC−26
Combination index (CI)
ED
(E)
RB−low/negative PDA cells
% live
CI
PD−0223991 (μM)
0 0.9 1.9 3.75 7.5 15
Gemcitabine (μM)
0 100% 100% 103% 102% 93% 70%
2.5 83% 87% 86% 87% 81% 57%
1.05 1.00 1.29 1.17 0.91
5.0 71% 70% 71% 74% 74% 60%
1.69 1.72 1.72 1.26 1.14
10 51% 55% 58% 57% 58% 47%
1.40 1.44 1.42 1.05 1.05
20 43% 42% 46% 44% 52% 43%
1.23 1.28 1.25 1.36 1.30
40 42% 47% 45% 38% 50% 28%
1.72 1.59 1.25 2.27 1.13
TKCC−27
TKCC−06
TKCC−16
TKCC−23
KPC
Combination index (CI)
ED
(F)
Seed FUCCI-labelled PDCLs (TKCC−05/27)
Add GEM and/or PD−0332991
GEM
PD−0332991
Day 1 2 3 4 5 6 7 8 9 10
Collect
Harvest, stain and fix samples
Annexin V
DAPI
PFA
Analyse samples on cytometer
(G)
RB−high TKCC−05
3 d
4 d
7 d
10 d
Total apoptosis (%)
Vehicle
PD−0332991
GEM
GEM+ PD−0332991
(H)
RB−negative TKCC−27
10 d
Total apoptosis (%)
Vehicle
PD−0332991
GEM
GEM+ PD−0332991
(I)
Vehicle
PD−0332991
G0 9.4%
G1 37.5%
S/G2/M 22.6%
G1/S 19.1%
G0 34.3%
G1 26%
S/G2/M 15.6%
G1/S 19.5%
S/G2/M 4.1%
mKO2 (YG582/15-A)
mAG (B530/30-A)
(J)
RB−high TKCC−05
Cell cycle distribution(%)
Vehicle
PD−0332991
GEM
GEM+ PD−0332991
(K)
RB−negative TKCC−27
Cell cycle distribution(%)
Vehicle
PD−0332991
GEM
GEM+ PD−0332991
M
G2
G0
S
G1
G1/S
mKO2−/mAG−
G0 (mKO2++)
G1 (mKO2+)
G1/S (mKO2+/mAG+)
S/G2/M (mAG+)

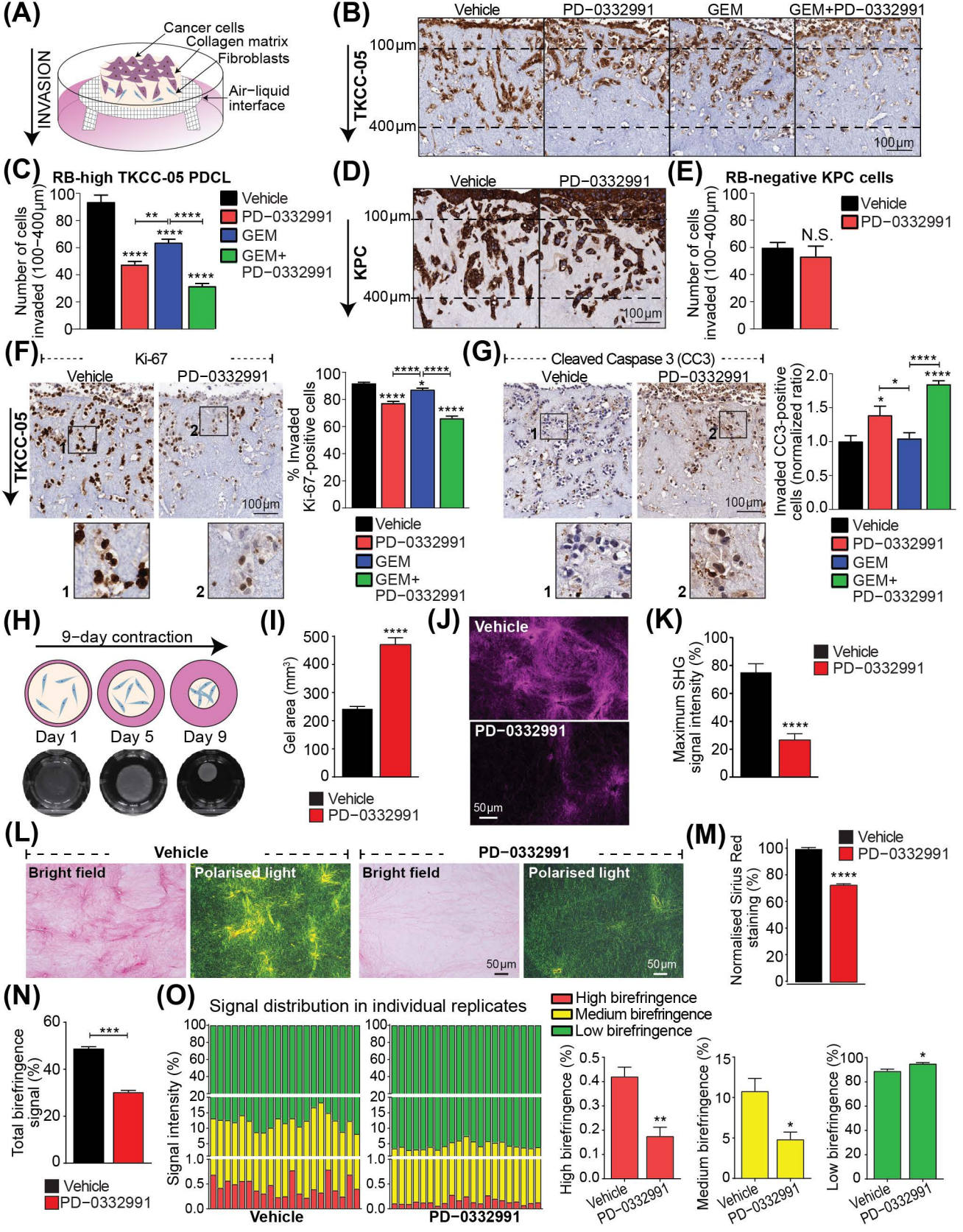
(A)
Cancer cells
Collagen matrix
Fibroblasts
Air–liquid interface
INVASION
(B)
Vehicle
PD–0332991
GEM
GEM+PD–0332991
TKCC-05
100μm
400μm
100μm
(C)
RB-high TKCC-05 PDCL
Number of cells invaded (100–400μm)
Vehicle
PD–0332991
GEM
GEM+ PD–0332991
(D)
Vehicle
PD–0332991
KPC
100μm
400μm
100μm
(E)
RB-negative KPC cells
Number of cells invaded (100–400μm)
N.S.
Vehicle
PD–0332991
(F)
Ki-67
Vehicle
PD–0332991
TKCC-05
100μm
% Invaded Ki-67-positive cells
Vehicle
PD–0332991
GEM
GEM+ PD–0332991
(G)
Cleaved Caspase 3 (CC3)
Vehicle
PD–0332991
100μm
Invaded CC3-positive cells (normalized ratio)
Vehicle
PD–0332991
GEM
GEM+ PD–0332991
(H)
9–day contraction
Day 1
Day 5
Day 9
(I)
Gel area (mm³)
Vehicle
PD–0332991
(J)
Vehicle
PD–0332991
50μm
(K)
Maximum SHG signal intensity (%)
Vehicle
PD–0332991
(L)
Vehicle
PD–0332991
Bright field
Polarised light
Bright field
Polarised light
50μm
50μm
(M)
Normalised Sirius Red staining (%)
Vehicle
PD–0332991
(N)
Total birefringence signal (%)
Vehicle
PD–0332991
(O)
Signal distribution in individual replicates
High birefringence
Medium birefringence
Low birefringence
Signal intensity (%)
Vehicle
PD–0332991
High birefringence (%)
Medium birefringence (%)
Low birefringence (%)
Vehicle
PD–0332991

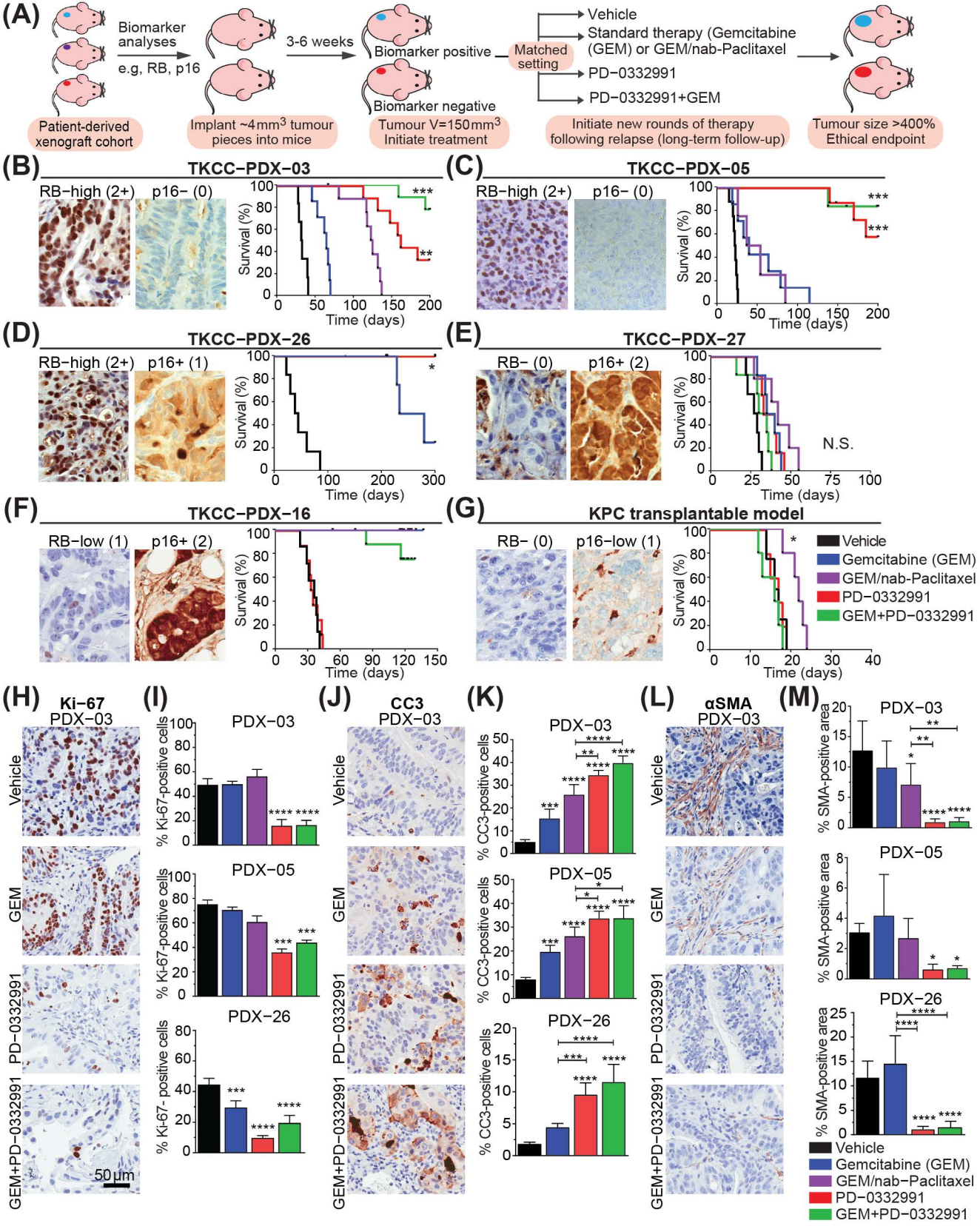
(A)
Biomarker analyses
e.g, RB, p16
3-6 weeks
Biomarker positive
Biomarker negative
Matched setting
Vehicle
Standard therapy (Gemcitabine (GEM) or GEM/nab-Paclitaxel
PD−0332991
PD−0332991+GEM
Patient-derived xenograft cohort
Implant ~4mm3 tumour pieces into mice
Tumour V=150mm3 Initiate treatment
Initiate new rounds of therapy following relapse (long-term follow-up)
Tumour size >400% Ethical endpoint
(B)
TKCC−PDX−03
RB−high (2+)
p16− (0)
Survival (%)
Time (days)
(C)
TKCC−PDX−05
RB−high (2+)
p16− (0)
Survival (%)
Time (days)
(D)
TKCC−PDX−26
RB−high (2+)
p16+ (1)
Survival (%)
Time (days)
(E)
TKCC−PDX−27
RB− (0)
p16+ (2)
N.S.
Survival (%)
Time (days)
(F)
TKCC−PDX−16
RB−low (1)
p16+ (2)
Survival (%)
Time (days)
(G)
KPC transplantable model
RB− (0)
p16−low (1)
Survival (%)
Time (days)
Vehicle
Gemcitabine (GEM)
GEM/nab−Paclitaxel
PD−0332991
GEM+PD−0332991
(H)
Ki−67
PDX−03
Vehicle
GEM
PD−0332991
GEM+PD−0332991
50 µm
(I)
PDX−03
PDX−05
PDX−26
% Ki-67-positive cells
% Ki-67- positive cells
(J)
CC3
PDX−03
Vehicle
GEM
PD−0332991
GEM+PD−0332991
(K)
PDX−03
PDX−05
PDX−26
% CC3-positive cells
(L)
αSMA
PDX−03
Vehicle
GEM
PD−0332991
GEM+PD−0332991
(M)
PDX−03
PDX−05
PDX−26
% SMA-positive area
Vehicle
Gemcitabine (GEM)
GEM/nab−Paclitaxel
PD−0332991
GEM+PD−0332991

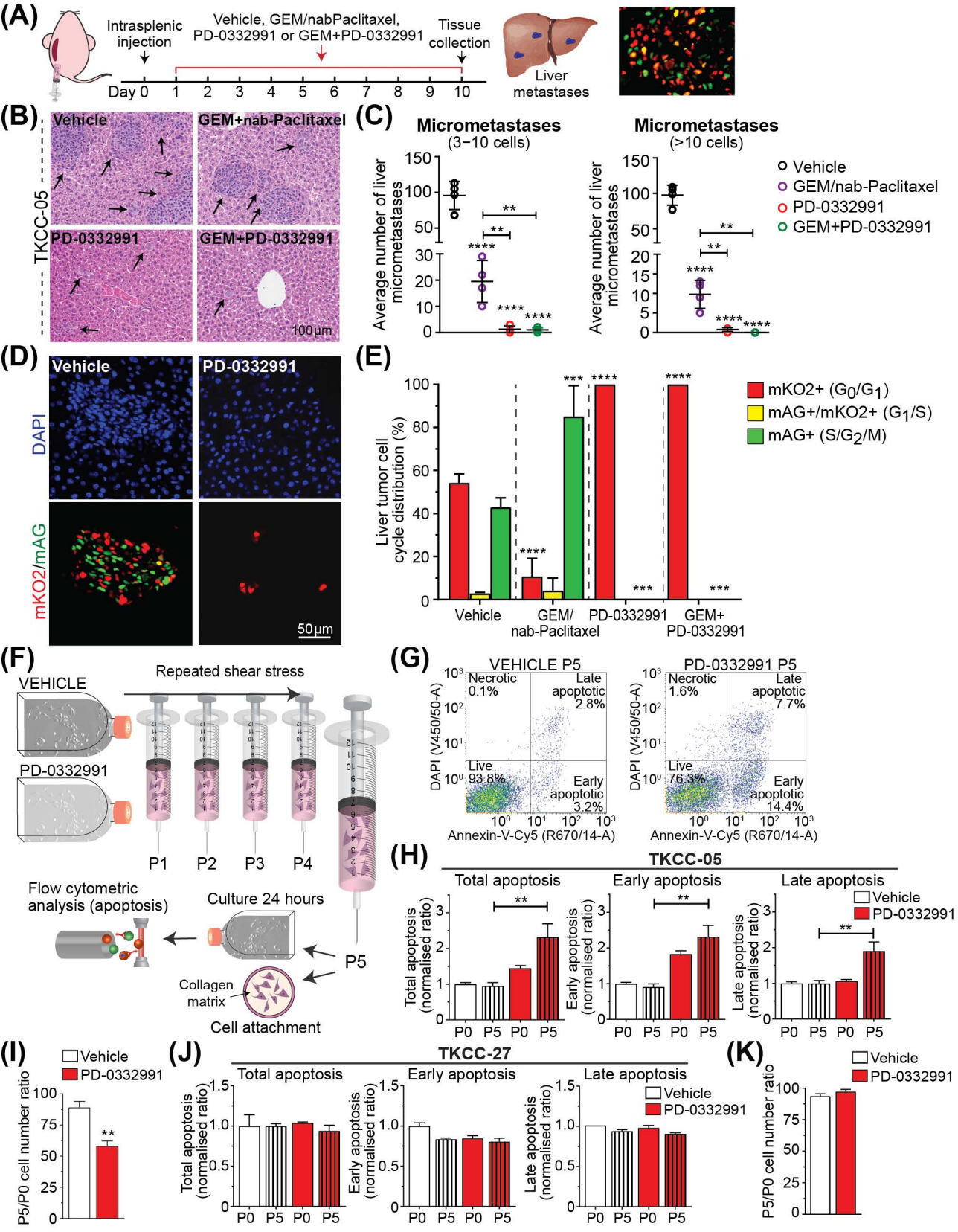
(A)
Intrasplenic injection
Vehicle, GEM/nabPaclitaxel, PD-0332991 or GEM+PD-0332991
Tissue collection
Day 0 1 2 3 4 5 6 7 8 9 10
Liver metastases
(B)
TKCC-05
Vehicle
GEM+nab-Paclitaxel
PD-0332991
GEM+PD-0332991
100μm
(C)
Micrometastases (3−10 cells)
Micrometastases (>10 cells)
Average number of liver micrometastases
Vehicle
GEM/nab-Paclitaxel
PD-0332991
GEM+PD-0332991
(D)
Vehicle
PD-0332991
DAPI
mKO2/mAG
50μm
(E)
Liver tumor cell cycle distribution (%)
mKO2+ (G0/G1)
mAG+/mKO2+ (G1/S)
mAG+ (S/G2/M)
Vehicle
GEM/ nab-Paclitaxel
PD-0332991
GEM+ PD-0332991
(F)
VEHICLE
PD-0332991
Repeated shear stress
P1
P2
P3
P4
P5
Flow cytometric analysis (apoptosis)
Culture 24 hours
Collagen matrix
Cell attachment
(G)
VEHICLE P5
PD-0332991 P5
Necrotic 0.1%
Late apoptotic 2.8%
Live 93.8%
Early apoptotic 3.2%
Necrotic 1.6%
Late apoptotic 7.7%
Live 76.3%
Early apoptotic 14.4%
DAPI (V450/50-A)
Annexin-V-Cy5 (R670/14-A)
(H)
TKCC-05
Total apoptosis
Early apoptosis
Late apoptosis
Total apoptosis (normalised ratio)
Early apoptosis (normalised ratio)
Late apoptosis (normalised ratio)
Vehicle
PD-0332991
P0 P5 P0 P5
(I)
Vehicle
PD-0332991
P5/P0 cell number ratio
(J)
TKCC-27
Total apoptosis
Early apoptosis
Late apoptosis
Vehicle
PD-0332991
(K)
Vehicle
PD-0332991
P5/P0 cell number ratio

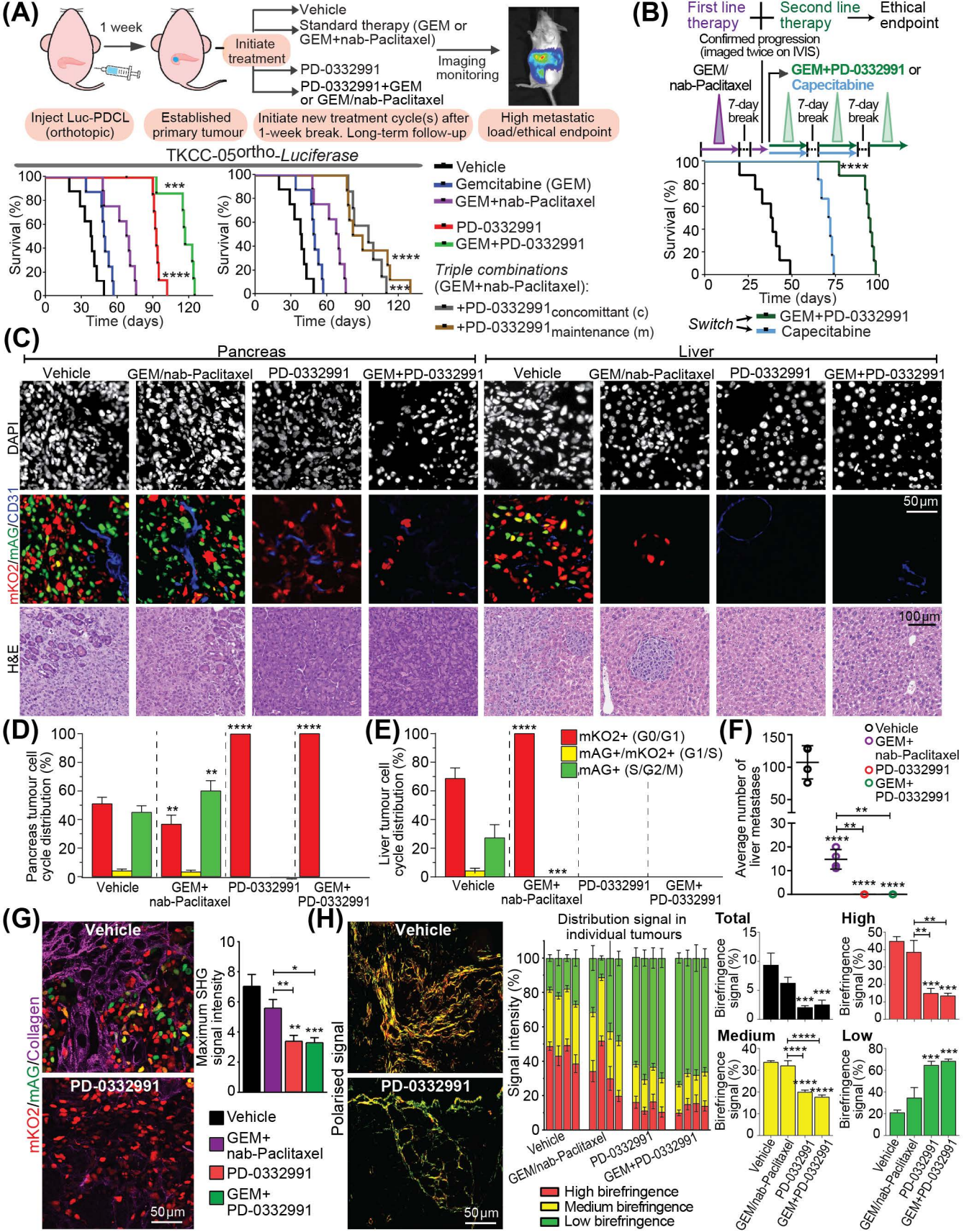
(A)
1 week
Initiate treatment
Vehicle
Standard therapy (GEM or GEM+nab-Paclitaxel)
PD-0332991
PD-0332991+GEM or GEM/nab-Paclitaxel
Imaging monitoring
Inject Luc-PDCL (orthotopic)
Established primary tumour
Initiate new treatment cycle(s) after 1-week break. Long-term follow-up
High metastatic load/ethical endpoint
TKCC-05ortho-Luciferase
Survival (%)
Time (days)
Vehicle
Gemcitabine (GEM)
GEM+nab-Paclitaxel
PD-0332991
GEM+PD-0332991
Triple combinations (GEM+nab-Paclitaxel):
+PD-0332991concomittant (c)
+PD-0332991maintenance (m)
(B)
First line therapy
Second line therapy
Ethical endpoint
Confirmed progression (imaged twice on IVIS)
GEM/ nab-Paclitaxel
GEM+PD-0332991 or Capecitabine
7-day break
Survival (%)
Time (days)
Switch
GEM+PD-0332991
Capecitabine
(C)
Pancreas
Liver
Vehicle
GEM/nab-Paclitaxel
PD-0332991
GEM+PD-0332991
DAPI
mKO2/mAG/CD31
H&E
50μm
100μm
(D)
Pancreas tumour cell cycle distribution (%)
Vehicle
GEM+ nab-Paclitaxel
PD-0332991
GEM+ PD-0332991
(E)
Liver tumour cell cycle distribution (%)
mKO2+ (G0/G1)
mAG+/mKO2+ (G1/S)
mAG+ (S/G2/M)
(F)
Average number of liver metastases
Vehicle
GEM+ nab-Paclitaxel
PD-0332991
GEM+ PD-0332991
(G)
Vehicle
PD-0332991
mKO2/mAG/Collagen
50μm
Maximum SHG signal intensity
Vehicle
GEM+ nab-Paclitaxel
PD-0332991
GEM+ PD-0332991
(H)
Vehicle
PD-0332991
Polarised signal
50μm
Distribution signal in individual tumours
Signal intensity (%)
Vehicle
GEM/nab-Paclitaxel
PD-0332991
GEM+PD-0332991
High birefringence
Medium birefringence
Low birefringence
Total
High
Medium
Low
Birefringence signal (%)

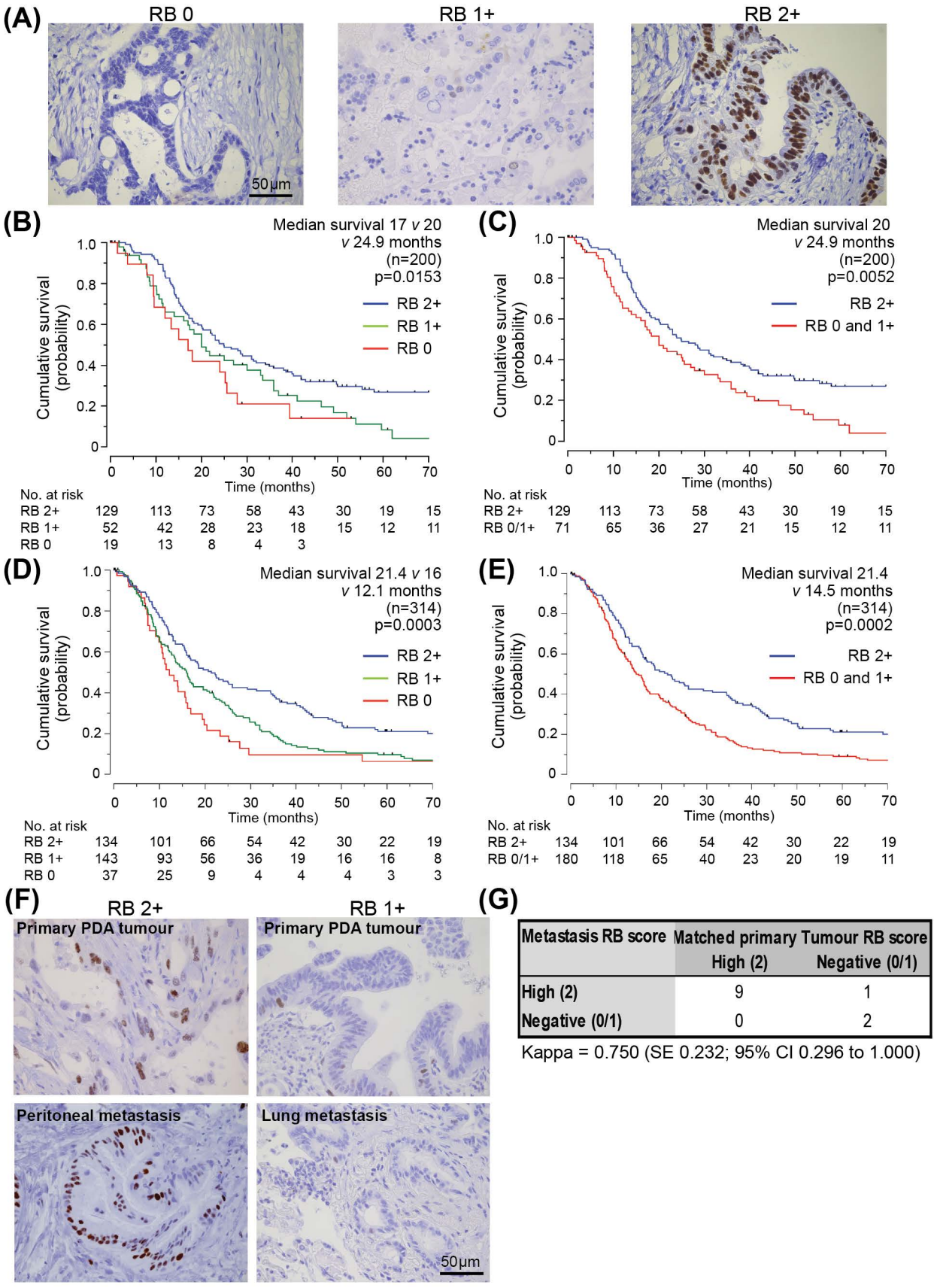

(G)

Metastasis RB score	Matched primary Tumour RB score	
	High (2)	Negative (0/1)
High (2)	9	1
Negative (0/1)	0	2

Kappa = 0.750 (SE 0.232; 95% CI 0.296 to 1.000)

SUPPLEMENTARY FILE 2

Supplementary Materials and Methods

Patient Cohort Information

APGI cohort: A cohort of 200 patients was utilized for clinico-pathological analysis, where 199 had primary operable, untreated PDA and underwent a pancreatectomy, and one patient had metastatic disease. 180 patients had a non-specific PDA type and 20 had rare histological subtypes. **NSWPCN cohort**: An additional cohort of 365 patients with operable PDA who underwent pancreatectomy was utilized for biomarker validation, with materials acquired from eight teaching hospitals associated with the NSWPCN. Fifty one patients were subsequently excluded from analysis due to lack of tumor material on tissue microarray. **RNSH metastatic set**: The pathology database of the Royal North Shore Hospital (RNSH), Sydney, Australia was searched for all metastatic PDAs biopsied from 2013 to June 2017. This center is a dedicated pancreatic cancer surgery unit and referral center for four community hospitals, hence the cohort represents a true snapshot of metastatic PDAs encountered in the community. RB expression was assessed on FFPE sections of metastatic PDAs and the samples included excision or core biopsies of mostly liver, peritoneum and omentum. Selected samples were biopsies or cytology specimens from the vertebra, brain and lung. Matched primary tumours if available were also assessed for RB expression on FFPE section and the samples included Whipple's resections and one fine needle aspiration from the pancreas.

Patient-Derived Cell Line (PDCL) Culture Conditions

All PDCLs were derived from patient-derived tumors initially established in immunocompromised mice, which were subsequently mechanically and enzymatically dissociated using collagenase (Stem Cell Technologies, US) and plated onto flasks coated with 0.2mg/ml−1 rat tail collagen (BD Biosciences, US). Epithelial cultures were enriched and purified using a FACS Aria III Cell sorter (BD Biosciences, US), using a biotinylated anti-mouse MHCI antibody (1:200 dilution; eBiosciences, US) coupled with Streptavidin AlexaFluor 647 secondary step (1:1,000; Invitrogen, US) and anti-mouse CD140a-PE antibody (1:300; BD Biosciences, US) to remove mouse stroma, as previously described[1]. Various PDCLs were cultured under the following conditions:

- TKCC-02, TKCC-03 and TKCC-04 in RPMI-1640 medium (Thermo Fisher Scientific, AU) supplemented with fetal bovine serum (10%) and 20ng/mL human recombinant epidermal growth factor (Thermo Fisher Scientific, AU).
- TKCC-05 and TKCC-06 PDCLs in a 1:1 mixture of Dulbecco's modified Eagle's medium and Ham's F12 medium (Thermo Fisher Scientific, AU) supplemented with fetal bovine serum (7.5%), 15mM HEPES (Thermo Fisher Scientific, AU), 1.2% Glucose 25ug/mL apo-transferrin, 40ng/ml hydrocortisone (Sigma-Aldrich, US), 0.1IU/mL insulin (Novo Nordisk, DK) and 10ng/ml human recombinant epidermal growth factor.
- TKCC-07, TKCC-09, TKCC-10, TKCC-12, TKCC-14, TKCC-15, TKCC-16, TKCC-17, TKCC-23, TKCC-26 and TKCC-27 in a 1:1 mixture of M199 medium and Ham's F12 medium (Thermo Fisher Scientific, AU) supplemented with fetal bovine serum (7.5%), 1x MEM vitamins, 2mM Glutamine (Thermo Fisher Scientific, AU), 15mM HEPES, 0.06% Glucose, 25ng/mL apo-transferrin, 0.2IU/mL insulin, 40ng/ml hydrocortisone, 20ng/ml epidermal growth factor, 0.5pg/mL Tri-iodothyronine, and 2ug/mL O-phosphoryl ethanolamine (Sigma-Aldrich, US).

- TKCC-18, TKCC-19 and TKCC-22 in IMDM medium (Thermo Fisher Scientific, AU) supplemented with fetal bovine serum (20%), 12.5ug/mL apo-transferrin, 0.2IU/mL insulin, 20ng/ml epidermal growth factor and 0.5x MEM vitamins.

Primary murine PDA cells from the genetically-engineered Pdx1-Cre, LSL-$Kras^{G12D/+}$, LSL-$Trp53^{R172H/+}$ (KPC) model were kindly provided by Dr Jennifer Morton. Cells were maintained in DMEM (Thermo Fisher Scientific, AU) supplemented with fetal bovine serum (10%).[2-4]

Data and Resource (Cell Line) Repository Information

Mutation summary data for the patient-derived cell lines utilized in this study is derived from the sequencing information available through our Australian Pancreatic Cancer Genome Initiative project as part of the International Cancer Genome Consortium, freely downloadable through http://icgc.org/icgc/cgp/68/304/798. Relevant ICGC codes and mutation data are summarized in supplementary table S1 of the manuscript. Patient-derived cell lines are also available to researchers upon request through the APGI website:

http://www.pancreaticcancer.net.au/bioresource-pdcls

In vitro Cytotoxicity and Drug Combination Studies

Cells for cytotoxicity assays were seeded in a 96-well plate and 24h post-seeding, gemcitabine, PD-0332991, 5-fluorouracil, paclitaxel (Selleck Chemicals, US) or nab-Paclitaxel (Specialized Therapeutics, Australia) were added. Cell viability was measured at 96h with AlamarBlue® (Ex 530-560nm, Em 590nm; Life Technologies, AU) and IC_{50} values were calculated using GraphPad Prism (V7.0.1, GraphPad, US). Recent studies have suggested that CDK4/6i may antagonize the effect of chemotherapies that target the cell cycle machinery, particularly when administered concomitantly with the chemotherapeutic[5]. Hence, for *in vitro* synergy screens, gemcitabine, standard therapy in PDA, was added to the culture 24h prior to PD-0332991. Drug interactions were analyzed using CompuSyn (V3.0.1, ComboSyn, US) to generate a combination index (CI) value, where CI<1 indicates synergy, CI=1 additive effect and CI>1 indicates antagonism.

Western Blotting

Lysates for western blotting were generated by harvesting log-phase cells, washing twice in PBS and lysing at 4°C in lysis buffer [Glycerol (10%), $MgCl_2$ (0.03%), HEPES (1.2%), SAPP (1%), Triton (1%), NaCl (0.8%), NaF (0.4%), EGTA (0.04%)] supplemented with protease inhibitors [MG132 (21µM), Aprotinin (1.5µM), DTT (1µM) , Leupeptin (23µM), Sodium Vanadate (1mM), PMSF (1µM)]. Cell debris was removed via centrifugation and protein concentration quantified using a Pierce™ BCA assay kit (Thermo Fisher Scientific, AU). Samples (20µg total protein) were resolved by SDS-PAGE on a Bis-Tris gel (4-12%) followed by transfer to a PVDF (0.45µM) membrane (Life Technologies, AU). Membranes were blocked in 5% non-fat milk in TBS-T [NaCl (0.87%), Tris (0.12%), Tween®20 (0.1%)] followed by overnight primary antibody incubation at 4°C. Antibodies for RB (#544136), phosphorylated-RB-Ser780 (#9307), p16 (#4824), CDK4 (#3136), CDK6 (#DCS83), Cyclin D1 (#2922S), CDK2 (#2546) and phosphorylated-p53-Ser15 (#9284) were purchased from Cell Signaling Technologies (Genesearch, AU). Antibodies for phosphorylated-CDK2-Thr160 (SC-101656), p53 (DO-1:SC-126/Pab 1801:SC-98) and Cyclin E (SC-247) were purchased from Santa Cruz Biotechnology, US. Detection was performed using a HRP-conjugated

enhanced chemiluminescence-based system (Perkin-Elmer, AU) and relative protein expression was quantified using Image J2 Software (V1.51, NIH, US).

Generation of Stable FUCCI and Luciferase-Expressing PDCLs

Lentiviral particles were generated by transient transfection of HEK293T cells utilizing a third generation packaging system, as previously described[6]. $2x10^6$ HEK293T cells were seeded in a 10cm dish in DMEM supplemented with 10% FCS and after 24h were transfected with a mixture of construct plasmids [pMD.G (2.8µg), pMDLg/pRRE (4.5µg), pRSV-Rev (6.4µg)], 15µg of a transfer plasmid [eGFP-luciferase, mKO2-hCdt1(30/120) or mAG-hGeminin(1/110)] and Lipofectamine 2000®. 24h post-transfection, HEK293T media was replenished and 24h later viral particles were harvested by filtration through a 0.45µm filter. PDCLs were infected by adding an optimized lentivirus dilution to culture media for 48h. Cells were harvested, washed extensively and positive cells were selected via cell sorting on a FACS Aria III (BD Biosciences, US) (Supplementary Fig. S2). FUCCI PDCLs were generated by initial infection and sorting for mAG, followed by subsequent infection and sorting for mKO2. Schematic (supplementary figure S3A) illustrates the cell cycle phases indicated by FUCCI fluorescence oscillation (adapted from[7]). mKO2-hCdt1 (30/120) is expressed in G_1 nuclei (orange), whilst mAG-hGeminin (1/110) is expressed during $S/G_2/M$ phase (green). S phase cells express mAG and mKO2 simultaneously (appearing yellow). Non-dividing cells accumulate higher levels of mKO2, hence mKO2++ cells are considered quiescent (G_0).

Flow Cytometry: Cell Cycle Distribution and Apoptosis

FUCCI-transduced TKCC-05 and TKCC-27 cells were treated with gemcitabine (0.01µM), gemcitabine/nab-Paclitaxel (0.001µM/0.001µM), PD-0332991 (0.3µM or 1µM respectively) or a combination over 10 days. At selected time-points (3, 4, 7, 10 days) cells were harvested and washed twice in cold PBS (figure 1F). For cell cycle analysis, FUCCI-transduced cells were fixed in paraformaldehyde (2%) for 15min at 4°C, and stained with a DAPI (1µM)/Triton-X (0.1%) solution for 30 min at 37°C. For apoptosis analysis, unfixed cells were stained with Annexin V-Cy5 (1:500) (BioVision, US) and DAPI (1µM) in Annexin V binding buffer (BioVision, US) for 15 min at room temperature. Cells were washed with binding buffer and fixed with paraformaldehyde (2%) for 15 min at 4°C, followed by two further binding buffer washes. Flow cytometric analysis was performed within 3h of staining on a LSRII SORP (BD Biosciences, US). Data were analysed with Kaluza Analysis Software (Beckman Coulter, US). A minimum of 20,000 events were analyzed per sample.

Fluid Shear Stress Assay

TKCC-05 or TKCC-27 cells were treated with 0.3 or 1µM PD-0332991 respectively for 72h. Cells were subsequently harvested, resuspended at a concentration of $5x10^5$ cell/ml and subject to controlled fluid shear stress as previously described.[8] An aliquot of cells not subject to shear stress, “P0” was used as a control. The sample was subject to shear stress through a 30G needle five times at a constant flow rate of 100µL/sec that corresponded to a maximum shear force of 1950 dyn/cm^2 [8] and designated “P5”. Following shear stress cells were placed back into culture for 24h and then harvested and stained with Annexin V/DAPI as described above for apoptosis analyses. Alternatively, following shear stress cells were seeded into wells pre-coated with 40µg/ml rat tail collagen (BD Biosciences, US) and allowed to attach for 10 minutes prior to extensive washing with culture media (three times) as previously described.[9] Cells were allowed 24h to recover and

attachment was quantified using CellTiter 96® AQueous One Solution Cell Proliferation Assay (Sigma, AU).

Subcutaneous and Orthotopic (*In Vivo*) Therapeutic Studies

For subcutaneous treatment studies (illustrated in figure 3A), treatment commenced when tumors reached 150mm3 (100%), where each mouse was randomized into a treatment group: (a) gemcitabine 120mg/kg twice weekly intraperitoneally (IP) for 25 days, (b) PD-0332991 150mg/kg daily gavage for 21 days, (c) gemcitabine (120mg/kg) twice weekly IP and PD-0332991 (150mg/kg) daily gavage or (d) gemcitabine (70mg/kg) and nab-Paclitaxel (30mg/kg) twice weekly IP for 25 days. In the combination arm, PD-0332991 was administered from week 2 for 21 days, 24h post-chemotherapy. Tumor size was monitored twice weekly by calipers and tumor volume calculated using the formula 0.5× length× width^2. Measurement of long-term treatment response was based on our published work, [1 10-12] with a 14-day minimal recovery time before additional treatment cycles. To avoid cumulative treatment-related toxicity, additional treatment was not given after the recovery time when tumor responded (tumor size<100%; partial response). Treatment was only continued once tumor relapsed to its original size (100%). Animals were euthanized at ethical endpoint (tumor volume>400% or time>200 days) and tissues collected for analyses.

For orthotopic studies, 15,000 luciferase- or FUCCI- labelled PDCLs in 1:1 PBS:Matrigel™ (BD Biosciences, US) were injected into the pancreas of 6-8 week old Nod/Scid/IL-2Rγnull (NSG) mice. Mice were randomized into treatment groups as for subcutaneous studies at one week post-surgery. Treatment groups were: (a) gemcitabine 120mg/kg twice weekly intraperitoneally (IP) for 25 days, (b) PD-0332991 150mg/kg daily gavage for 21 days, (c) gemcitabine (120mg/kg) twice weekly IP and PD-0332991 (150mg/kg) daily gavage or (d) gemcitabine (70mg/kg) and nab-Paclitaxel (30mg/kg) twice weekly IP for 25 days. Tumor burden was monitored weekly by bioluminescent imaging and analyzed (IVIS Spectrum; Living Image Software, Perkin-Elmer, US). Two additional treatment arms were included, involving triple combination of gemcitabine (70mg/kg), nab-Paclitaxel (30mg/kg) twice weekly IP administered either concomitantly with PD-0332991 (100mg/kg) gavage from week 2 on a 5-day “on”, 5-day “off” schedule for 20 days, or with PD-0332991 administered as maintenance therapy by daily gavage after completion of gemcitabine/nab-Paclitaxel treatment. Mice were given a one week break between treatment cycles and were euthanized at ethical endpoint (extensive metastatic load, ascites), followed by tissue collection for further analyses. All tissues were collected as formalin-fixed and paraffin-embedded, snap-frozen and OCT cryoprotected material. Mice bearing FUCCI-labelled TKCC-05 tumors were culled at a 50 day timepoint, with the exception of vehicle controls that were culled prior due to a heavy tumor burden. To preserve FUCCI fluorescence, tissues were fixed in 4% PFA, cryoprotected in 20% sucrose and embedded in OCT as previously described.[7]

Intrasplenic Injection of Tumor Cells

For intrasplenic injection experiments, FUCCI-labelled TKCC-05 cells (4x10^5 cells/50 µL PBS) were injected into the spleens of NSG mice (anesthetized with isoflurane 3L, O_2 1 L/min, vacuum was used constantly to remove excess of O_2) as previously achieved.[12] Treatments commenced on day 1 post-surgery to mimic systemic CDK4 inhibition during metastatic spread of PDA cells. See figure 4 for treatment timeline. Mice were culled 10 days post injection and tissues collected in 4% PFA as described above. Liver metastases were visualised via haematoxylin and eosin staining in addition to FUCCI immunofluorescent imaging as described below.

Organotypic Invasion and Contraction Assays

Organotypic assays were conducted as previously described.[13-15] Briefly, rat tail collagen I solution was prepared from the extraction of tendons with 0.5mol/L acetic acid to a concentration of 2mg/ml. Telomerase immortalized fibroblasts (TIFs) (8.3 $x10^4$ cells) were embedded in a mix of 2.5ml of rat-tail collagen I. Once polymerized the matrices were allowed to contract in complete media for 14 days (until matrices reached ~1.5cm in diameter). Subsequently, $1x10^5$ luciferase-labelled RB+ TKCC-05 cells were seeded on top of the matrix and allowed to grow to confluence for 4 days. Matrices were then transferred onto metal grids and raised to an air-liquid interface, where KPC or TKCC-05 cell invasion occurred for 14 or 21 days respectively (media and drugs were replenished every 2 days) (figure 2F). For drug treatments, 0.01μM gemcitabine was added for 24h (on day 1), and was subsequently removed and followed immediately by 0.3μM PD-0332991 for the remaining 20 days. Following invasion, the matrices were fixed in 10% formalin and processed for histochemical analysis. Cell invasion was determined by counting GFP-positive cells between 100μm and 400μm within the matrix. 12 independent images were taken per condition for analysis (*n*=3 independent biological experiments).

Contraction assays were conducted by allowing TIF-embedded polymerized matrices to contract in complete media for 9 days (figure 2I). Treatment with vehicle or 0.3μM PD-0332991 commenced on day 0, with media and drug replenishment every 2 days. Following contraction, each matrix diameter was measured and collagen gel area was quantified using ImageJ2.

Second Harmonic Generation (SHG) Imaging

Second Harmonic Generation (SHG) analyses were conducted as previously described[12] on formalin-fixed organotypic matrices and 8μm thick orthotopic tumor sections. Briefly, 3 representative regions of interest were imaged over a 3D z-stack (80μm depth for organotypic matrix with z-step size of 2.52μm; 8μm depth for tumor tissue with z-step size of 1.51μm). SHG signal was acquired using a 25x 0.95NA water objective on an inverted Leica DMI 6000 SP8 confocal microscope. Excitation source was a Ti:Sapphire femtosecond laser cavity (Coherent Chameleon Ultra II), operating at 80 MHz tuned to a wavelength of 890nm for organotypic matrices or 880nm for tumor sections. RLD HyD detectors (440/20 and 435/40, respectively) were used to detect SHG signal intensity. SHG signal intensity was quantified in MATLAB (MathWorks, US) for each image or stack and the maximum for each treatment was plotted.

Polarized Light Microscopy and Analysis

4 μm sections of fixed samples were deparaffinized, rehydrated, and stained with 0.1% picrosirius red (Polysciences) for fibrillar collagen according to manufacturer's instructions. Polarized light images were then collected using an Olympus U-POT polarizer in combination with an Olympus U-ANT transmitted light analyzer fitted to the microscope. Quantitative intensity measurements of fibrillar collagen birefringent signal were carried out on polarized light images using ImageJ, with analysis performed as recently achieved[12]. For each polarized light image, Hue-Saturation-Balance (HSB) thresholding was applied, where 1≥H≤27 | 0≥S≤255 | 7≥B≤255 was used for red-orange (high birefringent) fibers, 28≥H≤54 | 0≥S≤255 | 7≥B≤255 for yellow (medium birefringent) fibers, and 55≥H≤100 | 0≥S≤255 | 7≥B≤255 for green (low birefringent) fibers. The relative area (as a % of total fibers [1≥H≤100 | 0≥S≤255 | 7≥B≤255]) was then calculated.

Immunofluorescence of FUCCI Mouse Tissues

Immunofluorescent imaging of FUCCI mouse tissues was performed on 4µm sections of PFA fixed OCT embedded frozen tissue mounted on SuperFrost slides (Menzel-Glaser, Braunschweig, DE). Images were taken on an Leica DMI 5500 microscope (Leica, DE) at a resolution of 1392 x 1040 µm using a 20x/0.50 objective on four channels [A4 (Ex360/40-Em470/40), L5 (Ex480/40-Em527/30), N3 (Ex546/12-Em600/40) and Y5 (Ex620/60-Em700/75)]. Image capture was automated using LAS X Software (Leica, DE) and analysis was performed using ImageJ2.

Cell Tracking and Migration Analysis

TKCC-05 cells were seeded in a 6-well plate at a low density (30,000 cells per well) and treated with gemcitabine (0.01µM) and/or PD-0332991 (0.3µM) as detailed (figure 2A). Cell tracking was performed by acquiring images every 20 min from 0h to 96h post-treatment using a DMI 6000 inverted microscope (Leica, DE) maintained in a heated chamber (37°C) with 5% CO_2 for optimal cell growth. Media and drug/s were replenished at 48h. Images were taken at a resolution of 1856 x 1387 µM using a 20x/0.40 objective on three channels [Brightfield, GFP (Ex470/40-Em525/50) and N3 (Ex546/12-Em600/40)]. Image capture was automated using LAS X Software (Leica, DE), cell tracking was performed using the manual tracking plugin in Image J2 and data were analyzed in GraphPad Prism. Migration of vehicle- and drug-treated FUCCI-transduced TKCC-05 cells was tracked over a 12h period using ImageJ2 software, from 12 to 24 hrs and 96 to 108 hrs post-treatment (4 day time-point). A minimum of 60 cells per treatment condition were analyzed, unless complete cell cycle phase-specific arrest was observed (supplementary figure S7E, <10 cells observed in G_1/S phase at both early and late timepoints, and S/G_2/M phase at late time-point post-PD-0332991 or GEM/ PD-0332991 treatment). Migration direction was reconfigured using the Chemotaxis Tool in ImageJ2 software and superimposed.

Immunohistochemistry on Patient Material

Immunohistochemistry was performed on formalin-fixed paraffin-embedded tissue microarrays from the APGI/ICGC and NSWPCN clinical cohorts (3 x 1mm tissue cores per tumor). RB antibody was used at 1:1000 dilution (G3-245, BD Pharmingen, US). Staining for p16 was performed using a diagnostic CINtec® p16 Kit (Roche, AU). Scoring was performed by a specialist pancreatic histopathologist blinded to the corresponding clinico-pathological or molecular data. Complete absence of nuclear staining was scored as negative (0), presence of weak nuclear staining in any percentage of cells as 1+, with the presence of moderate to strong nuclear staining scored as 2+.

Additional Immunohistochemical Analyses (PDX Cohorts and Organotypic Assays)

Immunohistochemistry was performed on 4µm sections of tissue mounted on SuperFrost slides (Menzel-Glaser, Braunschweig, DE). For phosphorylated RB (pRB) immunohistochemical staining, antigen retrieval was achieved by using the S2367 target retrieval solution (pH 6; Dako Corporation, AU) in a pressure cooker for 1 min, and staining was performed on a Dako Autostainer (Dako Corporation, AU). RB and p16 staining of PDX material was performed as above on human specimens. For Ki67 and Cleaved caspase-3, or Anti-alpha smooth muscle Actin staining, antigen retrieval was achieved by using an ER2 (pH 9) or ER1 (pH 6) solution respectively (Dako Corporation, AU) and staining performed on a Leica/Bond Max System (Leica, DE). The Envision+ Mouse/Rabbit detection system (K4063; Dako Corporation, AU) was used to visualize primary antibodies. Phosphorylated RB^{780} (J146-35) mouse primary antibody was purchased from BD

Pharmingen (AU) and diluted at 1:500. Ki67 (9106-S) rabbit primary antibody was purchased from Thermo Fisher Scientific (AU) and diluted at 1:400. Anti-alpha smooth muscle Actin (ab5694) primary antibody was purchased from abcam (UK) and diluted 1:800. Cleaved caspase-3 antibody was purchased from Cell Signaling Technologies (Genesearch, AU) and diluted 1:300.

To visualize invaded TKCC-05 tumor cells following organotypic invasion, 4µm sections of formalin-fixed paraffin embedded matrices containing eGFP-luciferase-labelled TKCC-05 cells were first incubated in antigen retrieval solution (pH 9; (Leica, DE)) for 30 min at 93°C. Sections were subsequently incubated with the polyclonal rabbit anti-GFP antibody (A111-22, Thermo Scientific, AU) at a 1:1000 dilution for 1h, followed by detection with staining performed on a Leica/Bond Max System (Leica, DE). Pancytokeratin antibody (Leica-Novostra, C11) was used to visualize invaded KPC cells following organotypic invasion as previously described[15-17]. Ki-67 staining of matrices was performed as above at a dilution of 1:500 (9106-S, Thermo Scientific, AU). Picrosirius red staining was performed as per manufacturer's instructions (Polysciences, US). MATLAB software was used to calculate intensity of collagen fibers.

Supplementary References

1. Waddell N, Pajic M, Patch AM, et al. Whole genomes redefine the mutational landscape of pancreatic cancer. *Nature* 2015;518(7540):495-501.
2. Hingorani SR, Petricoin EF, Maitra A, et al. Preinvasive and invasive ductal pancreatic cancer and its early detection in the mouse. *Cancer Cell* 2003;4(6):437-50.
3. Hingorani SR, Wang L, Multani AS, et al. Trp53R172H and KrasG12D cooperate to promote chromosomal instability and widely metastatic pancreatic ductal adenocarcinoma in mice. *Cancer Cell* 2005;7(5):469-83.
4. Morran DC, Wu J, Jamieson NB, et al. Targeting mTOR dependency in pancreatic cancer. *Gut* 2014;63(9):1481-9.
5. Franco J, Witkiewicz AK, Knudsen ES. CDK4/6 inhibitors have potent activity in combination with pathway selective therapeutic agents in models of pancreatic cancer. *Oncotarget* 2014;5(15):6512-25.
6. Dull T, Zufferey R, Kelly M, et al. A third-generation lentivirus vector with a conditional packaging system. *Journal of virology* 1998;72(11):8463-71.
7. Sakaue-Sawano A, Kurokawa H, Morimura T, et al. Visualizing spatiotemporal dynamics of multicellular cell-cycle progression. *Cell* 2008;132(3):487-98.
8. Barnes JM, Nauseef JT, Henry MD. Resistance to Fluid Shear Stress Is a Conserved Biophysical Property of Malignant Cells. *PLoS One* 2012;7(12)
9. Chen Y, Lu B, Yang Q, et al. Combined integrin phosphoproteomic analyses and small interfering RNA--based functional screening identify key regulators for cancer cell adhesion and migration. *Cancer Res* 2009;69(8):3713-20.
10. Pajic M, Iyer JK, Kersbergen A, et al. Moderate increase in Mdr1a/1b expression causes in vivo resistance to doxorubicin in a mouse model for hereditary breast cancer. *Cancer Res* 2009;69(16):6396-404.
11. Rottenberg S, Nygren AO, Pajic M, et al. Selective induction of chemotherapy resistance of mammary tumors in a conditional mouse model for hereditary breast cancer. *Proc Natl Acad Sci U S A* 2007;104(29):12117-22.
12. Vennin C, Chin VT, Warren SC, et al. Transient tissue priming via ROCK inhibition uncouples pancreatic cancer progression, sensitivity to chemotherapy, and metastasis. *Sci Transl Med* 2017;9(384)
13. Johnsson AK, Dai Y, Nobis M, et al. The Rac-FRET Mouse Reveals Tight Spatiotemporal Control of Rac Activity in Primary Cells and Tissues. *Cell Rep* 2014;6(6):1153-64.
14. Nobis M, McGhee EJ, Morton JP, et al. Intravital FLIM-FRET imaging reveals dasatinib-induced spatial control of src in pancreatic cancer. *Cancer Res* 2013;73(15):4674-86.

15. Timpson P, McGhee EJ, Morton JP, et al. Spatial regulation of RhoA activity during pancreatic cancer cell invasion driven by mutant p53. *Cancer Res* 2011;71(3):747-57.
16. Morton JP, Karim SA, Graham K, et al. Dasatinib inhibits the development of metastases in a mouse model of pancreatic ductal adenocarcinoma. *Gastroenterology* 2010;139(1):292-303.
17. Timpson P, McGhee EJ, Erami Z, et al. Organotypic collagen I assay: a malleable platform to assess cell behaviour in a 3-dimensional context. *Journal of visualized experiments : JoVE* 2011(56):e3089.
18. Pajic M, Blatter S, Guyader C, et al. Selected alkylating agents can overcome drug tolerance of G0-like tumor cells and eradicate BRCA1-deficient mammary tumors in mice. *Clinical cancer research* 2017
19. Rottenberg S, Jaspers JE, Kersbergen A, et al. High sensitivity of BRCA1-deficient mammary tumors to the PARP inhibitor AZD2281 alone and in combination with platinum drugs. *Proc Natl Acad Sci U S A* 2008;105(44):17079-84.

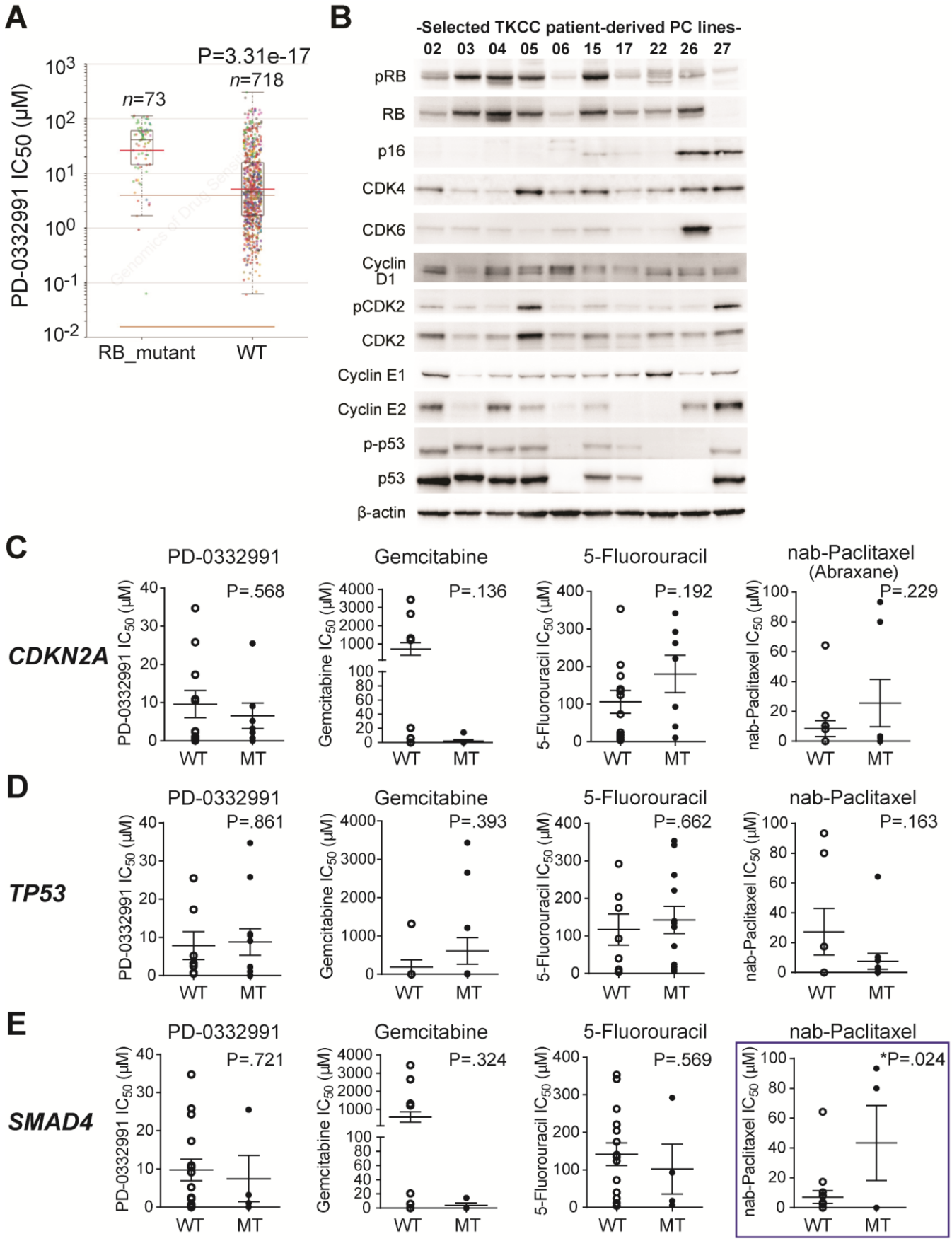

Supplementary Figure S1. **(A)** *RB1* gene mutations are associated with *in vitro* resistance to PD-0332991 (adapted from publically available datasets: www.cancerrxgene.org). **(B)** Baseline expression of key components of the CDK4/6 pathway and G_1/S cell cycle checkpoint in representative pancreatic PDCLs by western blot. Correlation analysis of PDCLs sensitivity to PD-0332991 and chemotherapeutics (gemcitabine, 5-Fluorouracil, nab-Paclitaxel) and basic mutation status: **(C)** (*CDKN2A*, **(D)** *TP53* and **(E)** *SMAD*4 mutations. *SMAD4* mutation (in *n*=4 PDCLs) was associated with significantly higher nab-Paclitaxel IC_{50}.

A TKCC-05 (RB-high)

% viability / CI index	Gemcitabine (nM)	PD-0223991 (μM) 0	0.13	0.25	0.5	1	2
	0	100.0%	82.1%	74.1%	73.0%	57.7%	54.1%
		-	± 2.6%	± 3.9%	± 1.1%	± 0.3%	± 0.9%
		-	-	-	-	-	-
	1.25	100.9%	80.8%	73.7%	68.5%	57.4%	53.1%
		± 4.3%	± 0.5%	± 2.3%	± 2.2%	± 5.5%	± 3.6%
		-	**0.88**	**0.78**	**0.91**	**0.70**	**0.96**
	2	98.3%	78.0%	72.0%	61.6%	56.0%	50.7%
		± 2.5%	± 3.4%	± 0.4%	± 1.9%	± 1.1%	± 6.1%
		-	**0.73**	**0.74**	**0.58**	**0.68**	**0.84**
	4	97.3%	74.3%	72.1%	61.5%	56.2%	50.5%
		± 1.0%	± 1.1%	± 2.9%	± 3.7%	± 1.2%	± 4.5%
		-	**0.66**	**0.86**	**0.67**	**0.78**	**0.91**
	7	92.8%	75.5%	66.1%	58.7%	54.6%	45.7%
		± 1.1%	± 8.8%	± 3.1%	± 2.9%	± 0.4%	± 1.5%
		-	**0.95**	**0.77**	**0.73**	**0.85**	**0.79**
	12	77.2%	62.9%	52.9%	49.7%	48.1%	40.6%
		± 1.4%	± 0.4%	± 5.2%	± 0.1%	± 1.6%	± 2.7%
		-	**0.84**	**0.70**	**0.73**	**0.84**	**0.80**

B TKCC-26 (RB-high, *CDK6* amplified)

% viability / CI index	Gemcitabine (nM)	PD-0223991 (μM) 0	1.8	2.6	4	6	12
	0	100.0%	98.8%	96.2%	96.4%	94.3%	70.4%
		-	± 5.1%	± 2.8%	± 4.2%	± 3.5%	± 0.1%
		-	-	-	-	-	-
	0.4	105.3%	95.0%	93.0%	90.6%	85.4%	64.4%
		± 1.6%	± 3.5%	± 0.6%	± 1.0%	± 6.0%	± 1.4%
		-	**0.53**	**0.61**	**0.74**	**0.83**	**0.98**
	0.9	99.3%	94.1%	93.6%	90.7%	84.9%	58.2%
		± 5.1%	± 4.0%	± 1.0%	± 7.7%	± 0.8%	± 4.5%
		-	**0.57**	**0.72**	**0.80**	**0.85**	**0.87**
	1.75	90.0%	91.1%	88.2%	87.7%	84.0%	57.2%
		± 3.5%	± 1.6%	± 1.1%	± 5.9%	± 3.1%	± 2.4%
		-	**0.55**	**0.58**	**0.76**	**0.88**	**0.87**
	3.5	89.9%	88.9%	88.3%	86.5%	82.5%	55.7%
		± 0.4%	± 6.5%	± 4.7%	± 1.6%	± 3.3%	± 1.7%
		-	**0.66**	**0.76**	**0.87**	**0.95**	**0.88**
	7	72.7%	70.7%	72.2%	71.9%	70.6%	55.7%
		± 0.9%	± 2.0%	± 2.5%	± 1.8%	± 4.2%	± 1.6%
		-	**0.42**	**0.52**	**0.63**	**0.77**	**0.96**

C TKCC-06 (RB-low)

% viability / CI index	Gemcitabine (μM)	PD-0223991 (μM) 0	0.5	0.9	1.9	3.75	7.5
	0	100.0%	96.4%	99.9%	98.7%	97.3%	92.8%
		-	± 7.3%	± 2.1%	± 0.8%	± 4.0%	± 4.4%
		-	-	-	-	-	-
	1.3	89.6%	96.7%	95.1%	97.2%	95.9%	94.0%
		± 1.2%	± 2.4%	± 2.6%	± 4.8%	± 1.1%	± 1.1%
		-	**1.01**	**0.85**	**1.53**	**1.60**	**1.88**
	2.5	87.6%	97.9%	92.4%	94.2%	96.5%	89.1%
		± 0.4%	± 2.3%	± 8.9%	± 4.8%	± 2.6%	± 3.6%
		-	**2.58**	**1.10**	**1.51**	**2.62**	**1.60**
	5.0	73.1%	87.1%	83.8%	81.5%	85.3%	75.2%
		± 3.9%	± 0.4%	± 3.9%	± 3.8%	± 4.9%	± 2.3%
		-	**1.34**	**1.16**	**1.11**	**1.51**	**1.21**
	10	71.7%	75.6%	78.6%	78.5%	76.9%	72.6%
		± 3.1%	± 1.2%	± 2.7%	± 4.8%	± 2.8%	± 3.6%
		-	**1.54**	**1.77**	**1.83**	**1.84**	**1.79**
	20	57.3%	62.8%	60.6%	61.0%	64.3%	64.3%
		± 3.6%	± 2.3%	± 5.1%	± 4.8%	± 5.0%	± 9.2%
		-	**2.02**	**1.91**	**1.97**	**2.26**	**2.43**

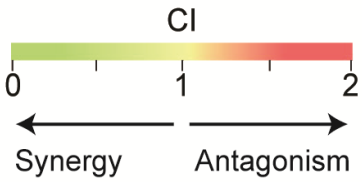

Supplementary Figure S2. Heat map showing cell viability and combination index (CI) values of gemcitabine and PD-0332991 efficacy examined in various chemotherapy/inhibitor ratios in additional **(A)** RB-high, **(B)** RB-high, *CDK6* amplified and **(C)** RB-low PDCLs. Data are representative of three independent experiments performed in triplicate.

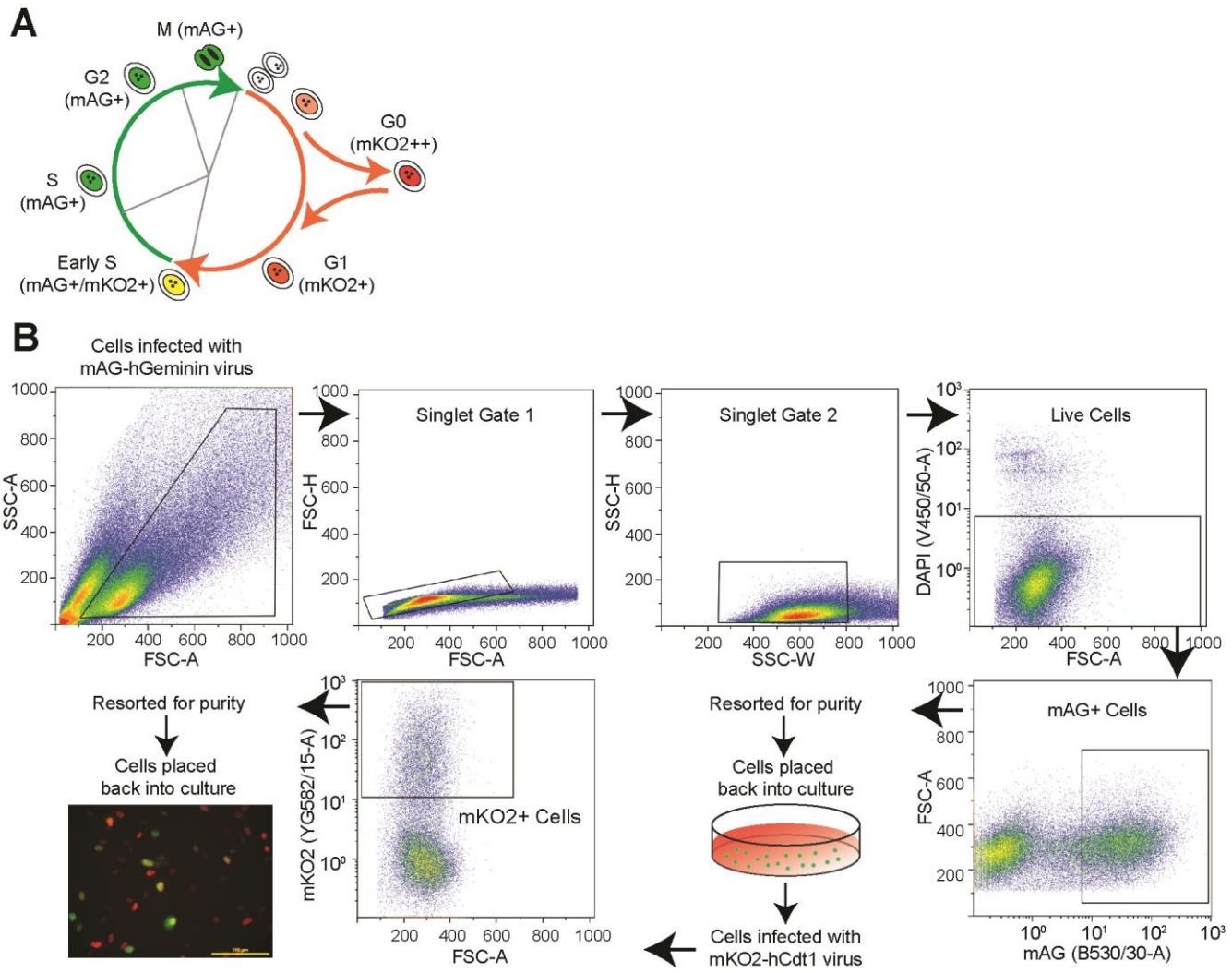

Supplementary Figure S3. Generation of stable FUCCI-expressing cell lines. **(A)** Schematic illustrating the cell cycle phases indicated by FUCCI fluorescence oscillation. mKO2-hCdt1 (30/120) is expressed in G_1 nuclei (orange), whilst mAG-hGeminin (1/110) is expressed during $S/G_2/M$ phase (green). S phase cells express mAG and mKO2 simultaneously (appearing yellow). Non-dividing cells accumulate higher levels of mKO2, hence mKO2++ cells are considered quiescent (G_0). Adapted from [7]. **(B)** Gating strategy for generation of cell lines stably expressing FUCCI. Cells were infected with mAG-hGeminin lentiviral particles for 48h before washing and FACS for single mAG positive cells (B530/30-A). Cells were placed back into culture, allowed to recover and subsequently infected with mKO2-hCdt1 lentiviral particles. Cells were washed and re-sorted using identical singlet gates to isolate single mKO2 (YG582/15-A) positive cells. After each single sort cells were re-sorted to ensure maximal purity (>99%).

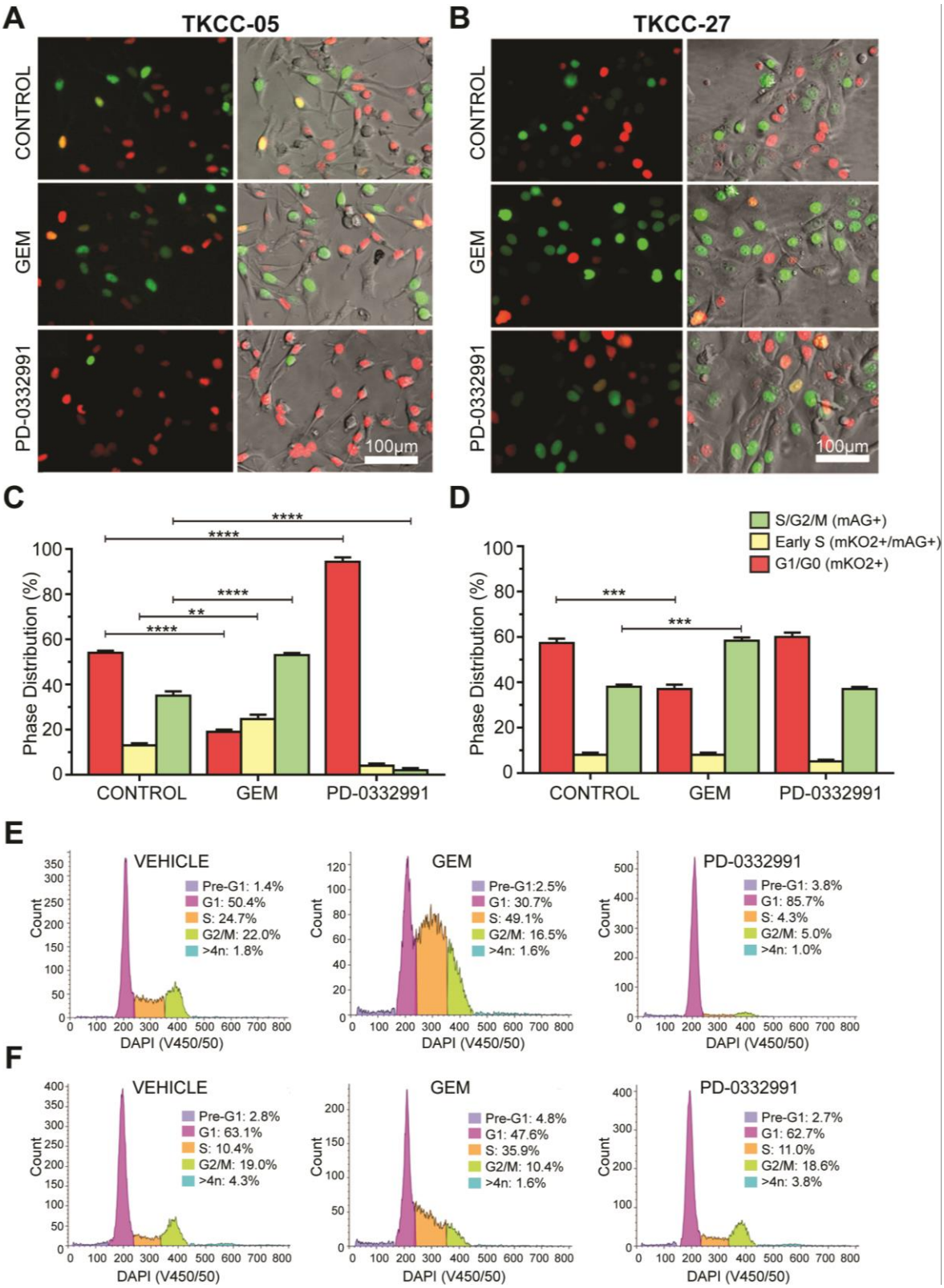

Supplementary Figure S4. **(A)** RB-positive FUCCI-transduced TKCC-05 cells and **(B)** RB-negative FUCCI-transduced TKCC-27 cells treated with gemcitabine (0.01µM) or PD-0332991 for 24h and imaged (Leica DM IL LED microscope). PD-0332991-sensitive TKCC-05 cells were treated with 0.3µM PD-0332991, whereas for the PD-0332991-resistant TKCC-27, 1µM concentration was used. *(Left)* green: Ex470/40-Em525/50, red: Ex560/40-Em645/75, *(Right)* overlay. Quantification of cell cycle distribution of **(C)** TKCC-05-FUCCI and **(D)** TKCC-27-FUCCI cells 24h post-treatment. Data shown as Mean ± SEM (n=3 independent experiments). PD-0332991 treatment (1 µM; 24 h) of FUCCI-transduced RB-negative TKCC-27 did not significantly alter the cell cycle distribution profile. Gemcitabine (GEM) treatment of the same PDCL, as anticipated, led to a significant increase in "green" cells which delineate S/G_2/M phase arrest. *(E, F)* Cell cycle phase distribution assayed by standard DAPI staining and flow cytometry analysis of **(E)** RB-positive TKCC-05 and **(F)** RB-negative TKCC-27 lines following treatment with GEM or PD-0332991.

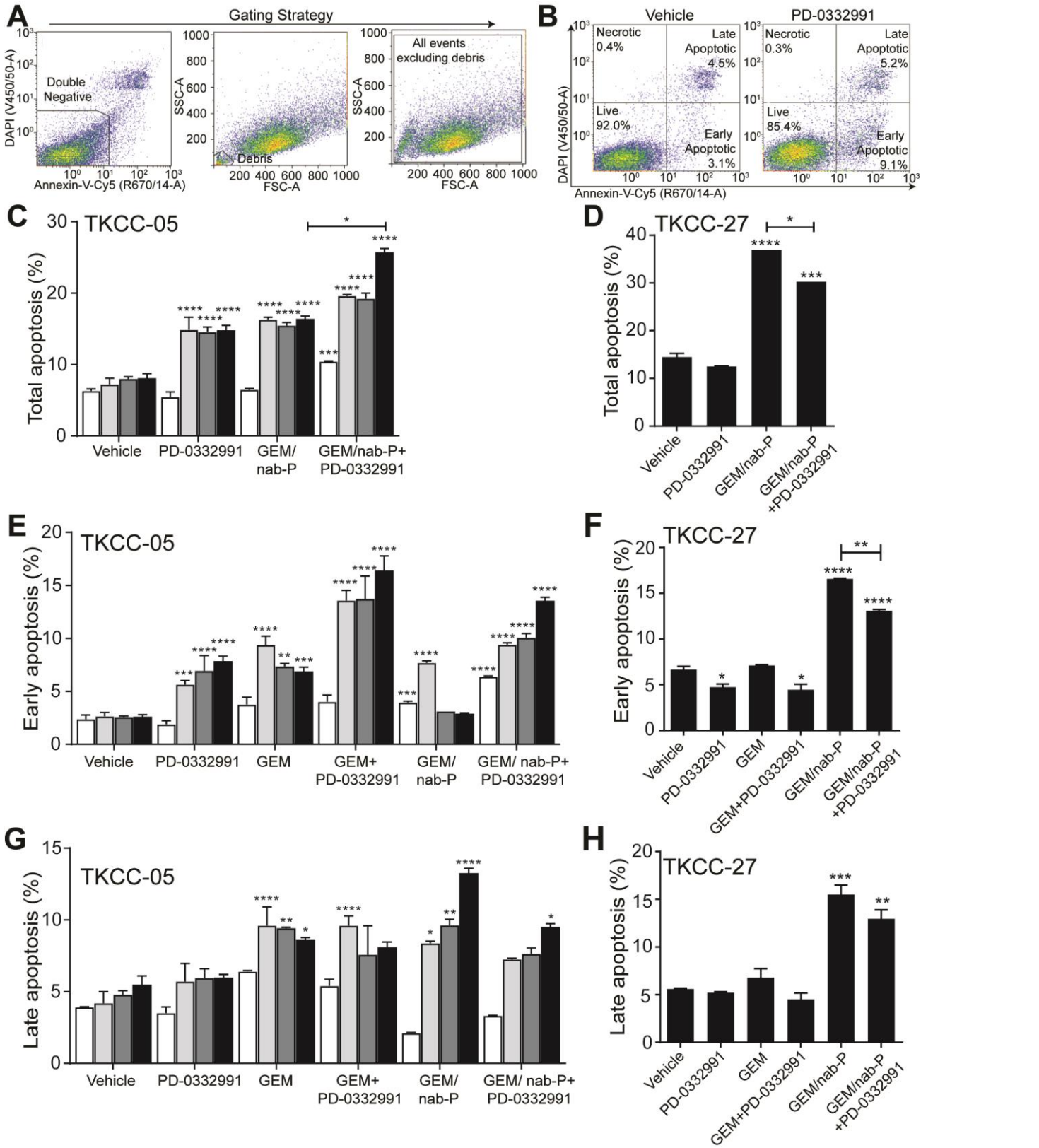

Supplementary Figure S5. Effect of PD-0332991-based therapeutic intervention on apoptosis in candidate FUCCI-transduced PDCLs. **(A)** Gating strategy for Annexin V-Cy5(R670/14-A)/ DAPI(V450/50-A) apoptosis analysis. The double negative (Annexin V-Cy5-/DAPI-) population was gated and displayed on a FSC-A/SSC-A plot where debris was excluded. A broad gate was then applied to all events excluding debris to ensure inclusion of shrunken dead and/or dying cells and to eliminate doublets and large cells. This gated population was then further analyzed. **(B)** Representative TKCC-05-FUCCI apoptosis plots and gating strategy post-treatment (10 days) and control. Total apoptosis quantified across all examined timepoints and gemcitabine (GEM)/nab-paclitaxel (nab-P)-based comparisons for **(C)** RB-high TKCC-05 and **(D)** RB-negative TKCC-27 cells. Quantified **(E-F)** early and **(G-H)** late apoptosis across all examined timepoints and treatments for **(E,G)** RB-high TKCC-05 and **(F,H)** RB-negative TKCC-27 cells. (mean ± SEM; *n*=4 independent experiments). Comparisons were performed against relevant vehicle controls, unless specified.

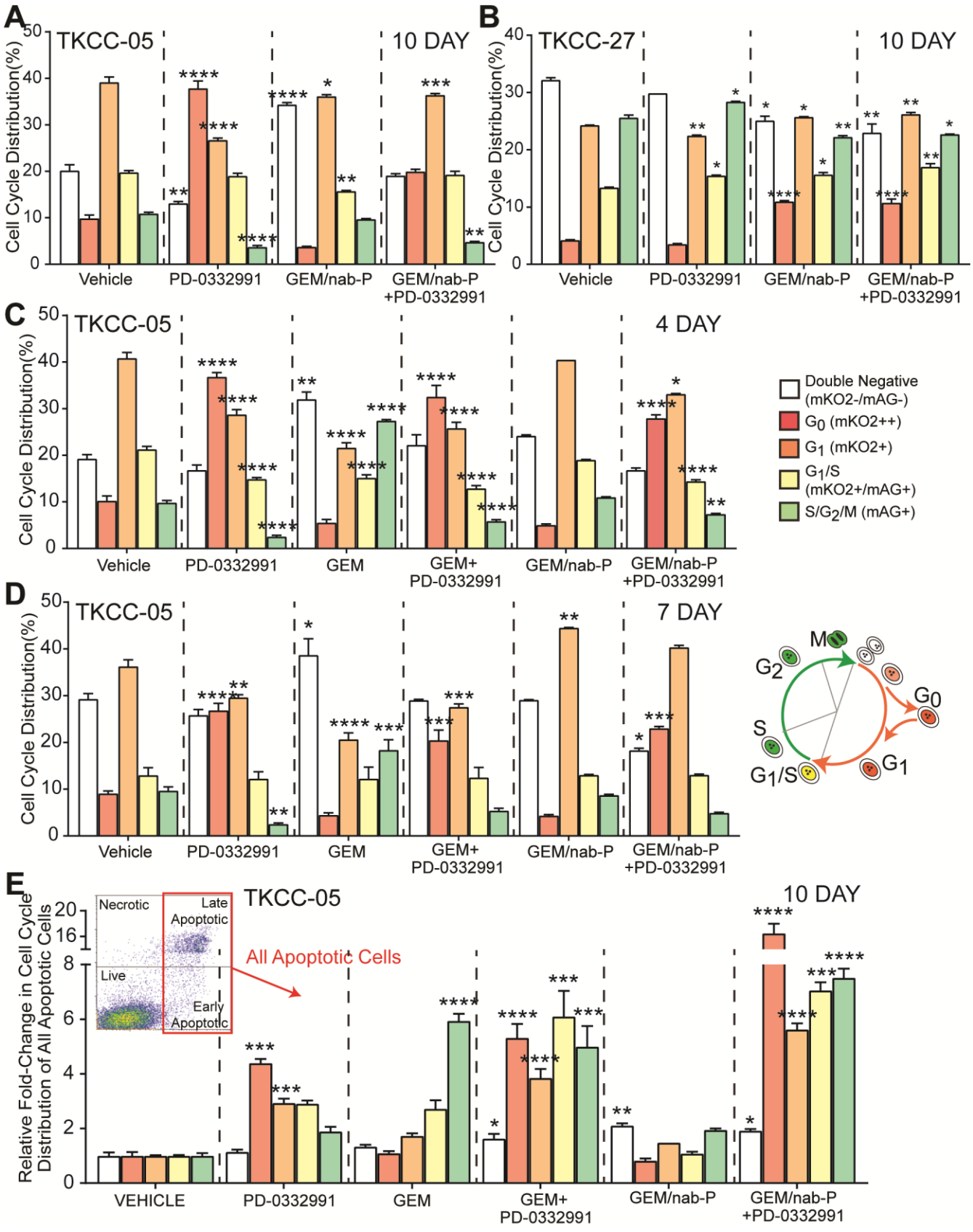

Supplementary Figure S6: Cell cycle distribution in candidate RB-high (TKCC-05) and RB-negative (TKCC-27) FUCCI-PDCLs following treatment with PD-0332991 (0.3μM and 1μM, respectively), gemcitabine (GEM; 0.01μM), GEM/nab-paclitaxel (nab-P; 0.001μM/0.001μM each) and combinations. Quantified cell cycle distribution following triple combination therapy (GEM/nab-P+PD-0332991), 10-days timepoint in **(A)** RB-high and **(B)** RB-negative PDCLs. Quantified cell cycle distribution across all examined treatments in RB-high TKCC-05, at earlier **(C)** 4-day and **(D)** 7-day timepoints. Cell cycle distribution in all apoptotic cells at **(E)** 10 days. Data shown as mean ± SEM (*n*=4 independent experiments). All comparisons were performed against the relevant vehicle controls, unless specified.

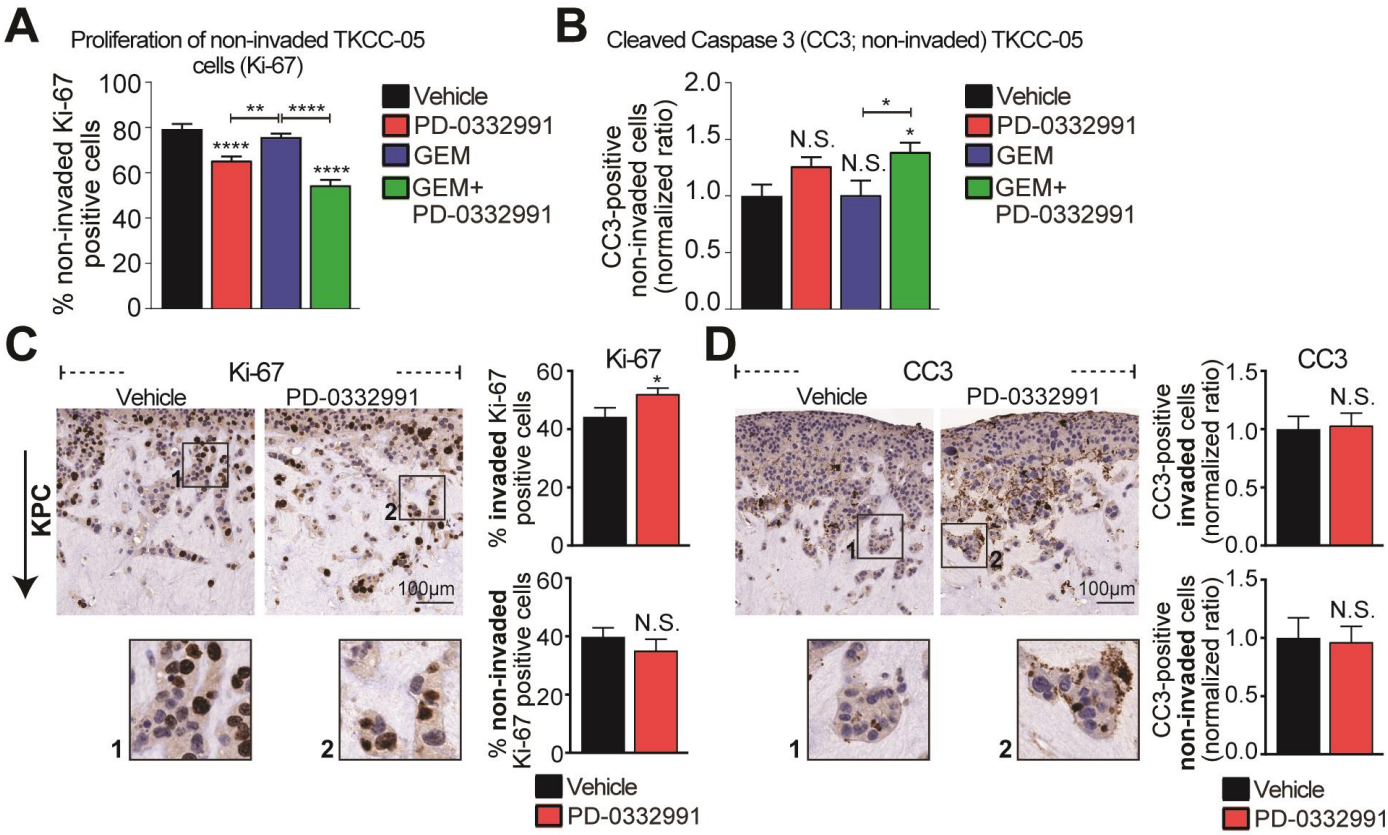

Supplementary Figure S7 The effect of PD-0332991 on the proliferative capacity and viability in selected pancreatic cancer lines in 3D. Quantification of **(A)** percentage Ki-67-positive and **(B)** apoptotic cleaved caspase 3 (CC3)- positive TKCC-05 cells in the non-invaded (top) fraction within organotypic matrices following therapeutic intervention with PD-0332991-based approaches (Fig 2F-G, Supplementary Materials and Methods). **(C)** Representative images of Ki-67 staining and quantification of the percentage Ki-67-positive KPC cells in organotypic matrices (invaded and non-invaded) post-PD-0332991 treatment. **(D)** Representative images of CC3 staining and quantification of KPC cells positive for CC3 (ratio normalized to control) in organotypic matrices (invaded and non-invaded) post-treatment.

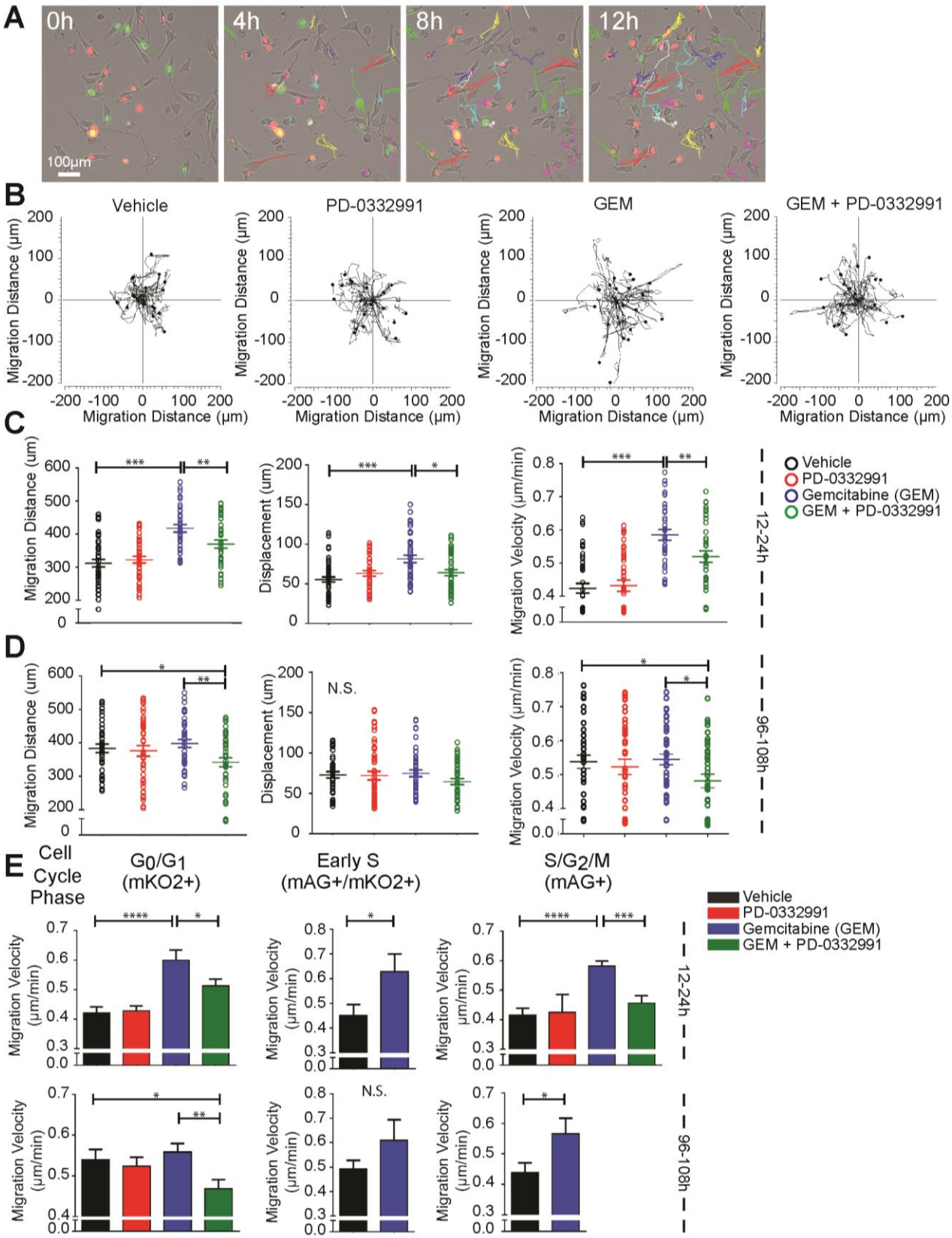

Supplementary Figure S8. Gemcitabine (GEM) and PD-0332991 combination inhibits migration in a RB-high PDCL. **(A)** Migration of vehicle-treated TKCC-05-FUCCI pancreatic cancer cells over a 12h period (20 min increments) tracked using manual tracking in ImageJ2. **(B)** Migration of vehicle- and drug-treated FUCCI-transduced TKCC-05 cells over a 12h period (12-24h post-treatment). For migration analysis, minimally 60 cells were chosen at random in each field, direction reconfigured using the Chemotaxis Tool in ImageJ2 software and superimposed (n=60). Migration distance *(left)*, displacement *(middle)* and velocity *(right)* quantified at **(C)** 12 to 24h post-treatment and **(D)** a 12h period 4 days post-treatment. (*n*=3 independent experiments; mean ± SEM). **(E)** Migration velocity data stratified into groups based on cell cycle phase for the same time periods respectively ***(C, D).*** In certain drug-treated conditions, cell cycle phase-specific arrest was efficient with no cells detected in other phases (<10 cells).

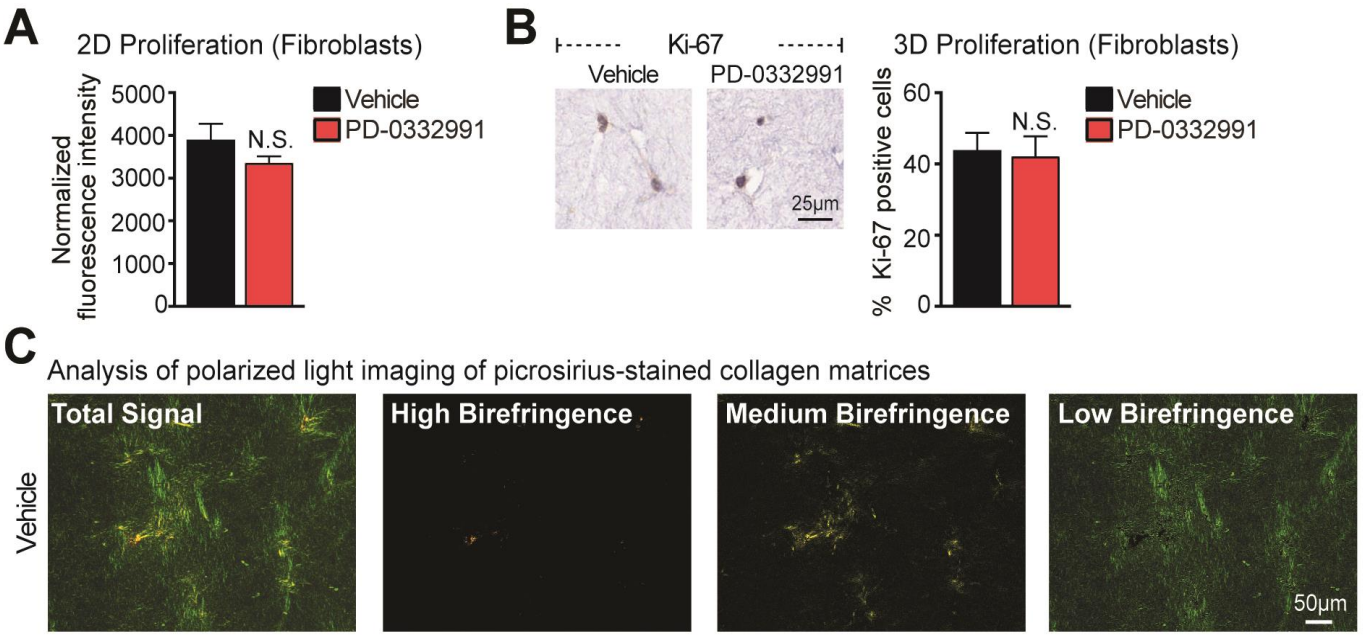

Supplementary Figure S9. The effect of PD-0332991 on the proliferative capacity and viability of fibroblasts in 2D and 3D. **(A)** AlamarBlue analysis of telomerase immortalized fibroblast (TIF) proliferation+/- PD-0332991 in 2D (72-hour assay). **(B)** Representative images of Ki-67 staining and quantification of TIF proliferation in collagen matrices after 9-day contraction assay +/- PD-0332991. Data shown as mean ± SEM (*n*=3 independent experiments, performed in triplicate matrices/ wells per condition, per repeat). All comparisons were performed against the relevant vehicle controls, unless specified. **(C)** Representative images of signal emitted from collagen fibres with high (red/orange), medium (yellow), and low (green) birefringence in collagen matrices stained with picrosirius red and imaged with polarized light microscopy.

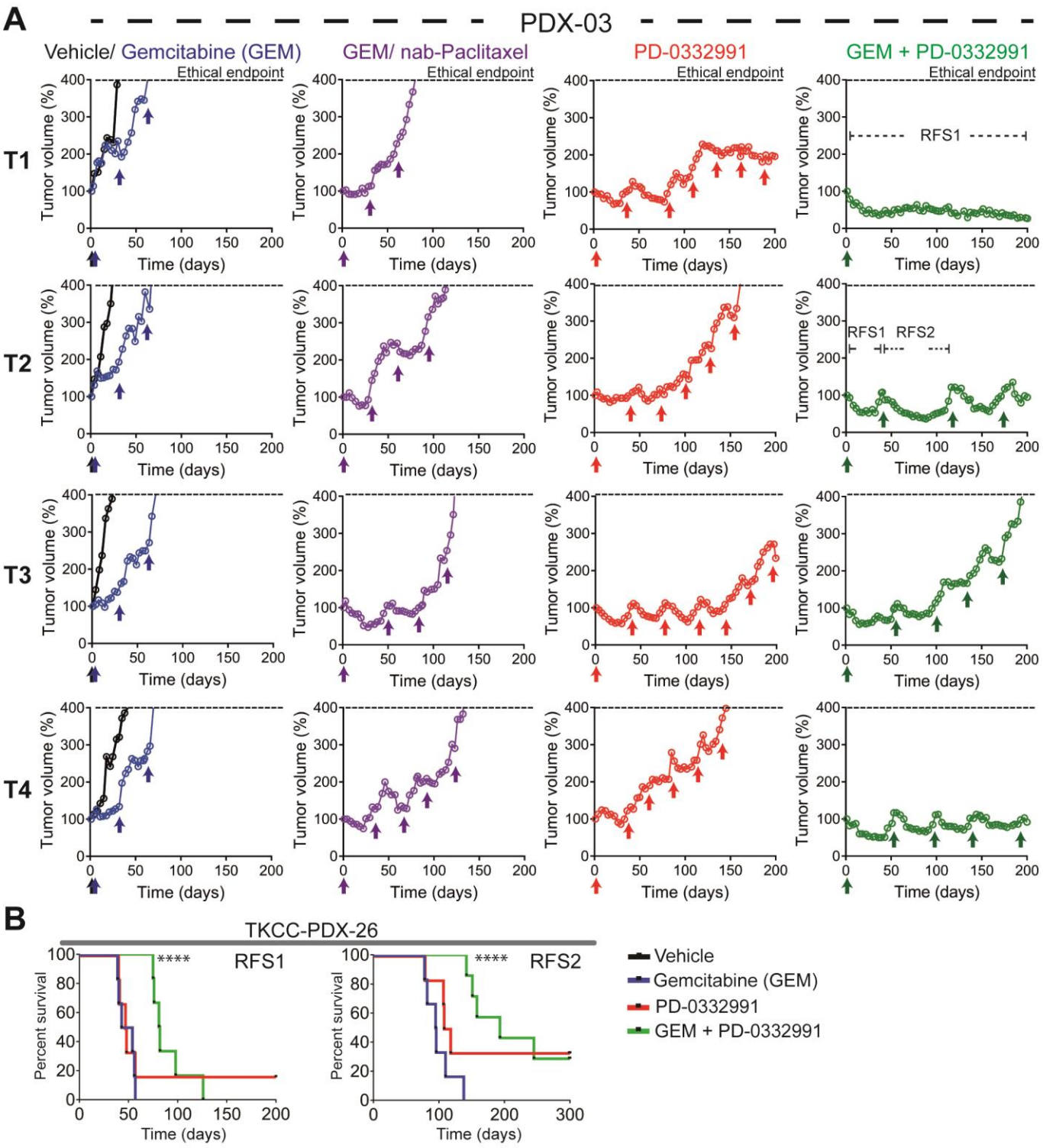

Supplementary Figure S10. Therapeutic response of RB-high PDXs to targeted therapy. **(A)** Representative responses of individual PDX-03 tumor grafts (T1-T4) to standard therapy and targeted treatments (PD-0332991 and combination). Small tumor fragments were transplanted subcutaneously into immunocompromised mice and treated with vehicle (black), 120mg/kg gemcitabine (GEM) intraperitoneally (IP) twice per week for 4 weeks (blue), 30mg/kg nab-Paclitaxel IP twice per week for four weeks in combination with 70mg/kg GEM (purple), 150mg/kg PD-0332991 daily oral gavage for 21 d as monotherapy (red) or in combination with unmodified GEM dose (green). Where tumors did not regress (tumor volume ≥100%), a new treatment cycle was initiated after a recovery time of two weeks (arrows). Treatment strategy as per Materials and Methods. **(B)** Increased relapse-free survival (RFS1 and RFS2) in RB-high, *CDK6*-amplified PDX-26 treated with GEM + PD-0332991 combination. RFS was defined as time between treatment cycles, as indicated in **(A)**, with each recurrence defined as re-growth of the tumor to the original starting volume of 100% (150mm3), as previously described [10 11 18 19]. Log rank analysis was used to compare efficacy of targeted approaches to standard therapy GEM.

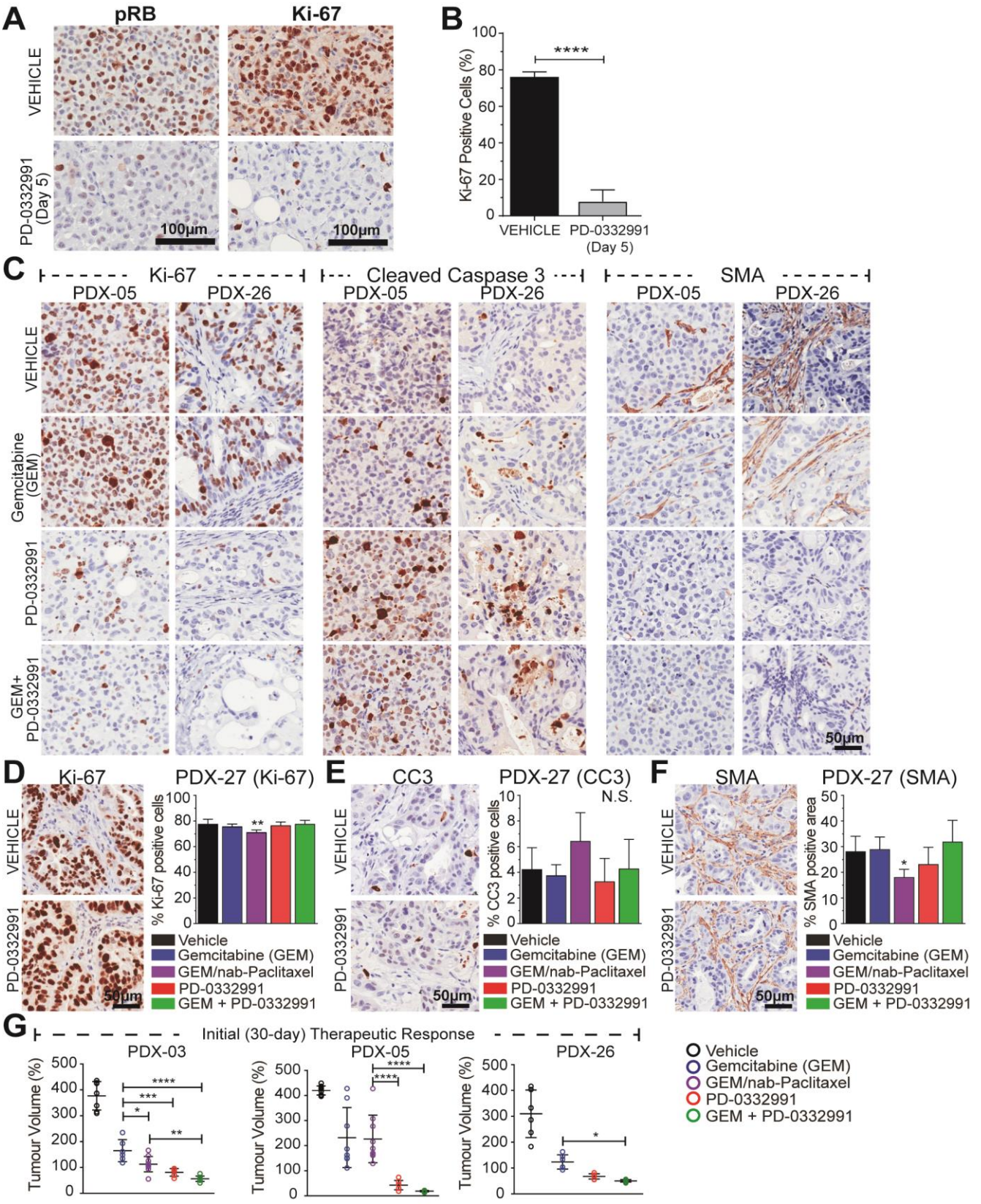

Supplementary Figure S11. PD-0332991 and gemcitabine (GEM)/ PD-0332991 combination treatment induces prolonged quiescence in tumor remnants and significant tumor shrinkage in RB-high PDA. **(A)** Levels of pRB and **(B)** proliferation measured by Ki-67 staining and **(C)** quantified following 5 days of daily treatment with PD-0332991 (150mg/kg) or vehicle of RB-high PDX-05 (*n*=4 mice per treatment group). **(C)** Representative images of Ki-67 (*left*), cleaved caspase 3 (CC3; *middle*) and alpha-smooth muscle actin (SMA; *right*) staining in PDX-05 and PDX-26 post-treatment (collected at endpoint). Representative images and quantitative analysis of RB-negative PDX-27 for **(D)** Ki-67 **(E)** CC3 and **(F)** SMA positivity following treatment. **(G)** Early treatment response in RB-high PDX-03 (*left*), PDX-05 (*middle*) and *CDK*6-amplified PDX-26 (*right*) to PD-0332991-based approaches, compared with standard-of-care treatments, 30 days post-initiation of therapy. Data shown as mean ± SD (n=6 to 8 mice minimally per treatment group).

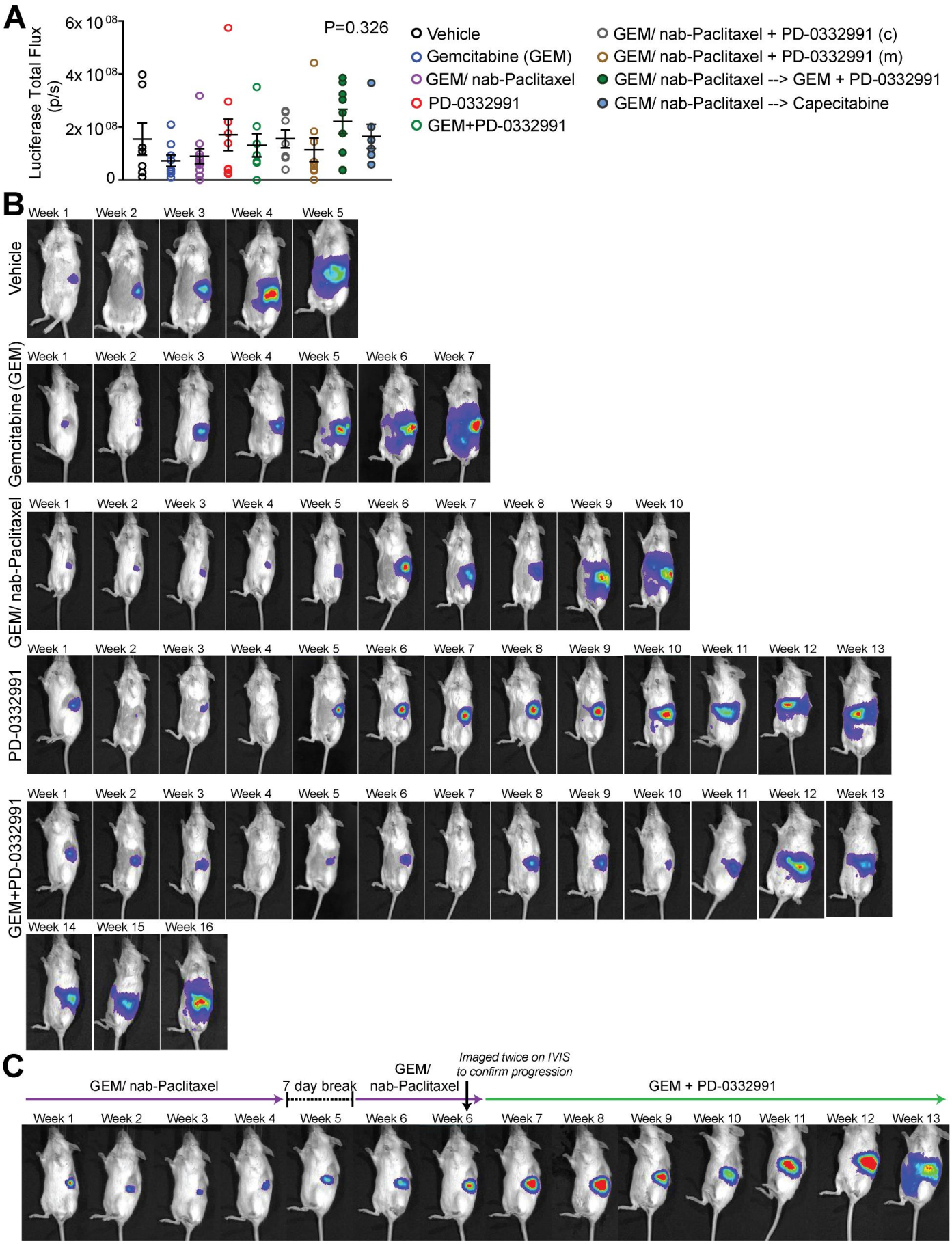

Supplementary Figure S12. **(A)** Analysis of Luciferase total flux (photons/sec) on day 7 post-injection of TKCC-05 PDCL shows no significant difference in tumor size once mice were randomized to treatment groups. **(B)** Whole-body imaging of mice bearing pancreatic Luciferase-transduced patient-derived tumors (TKCC-05^{ortho}-*Luciferase*) undergoing key treatments. **(C)** Outline and associated whole-body imaging for the set-up of the therapeutic switch experiment.

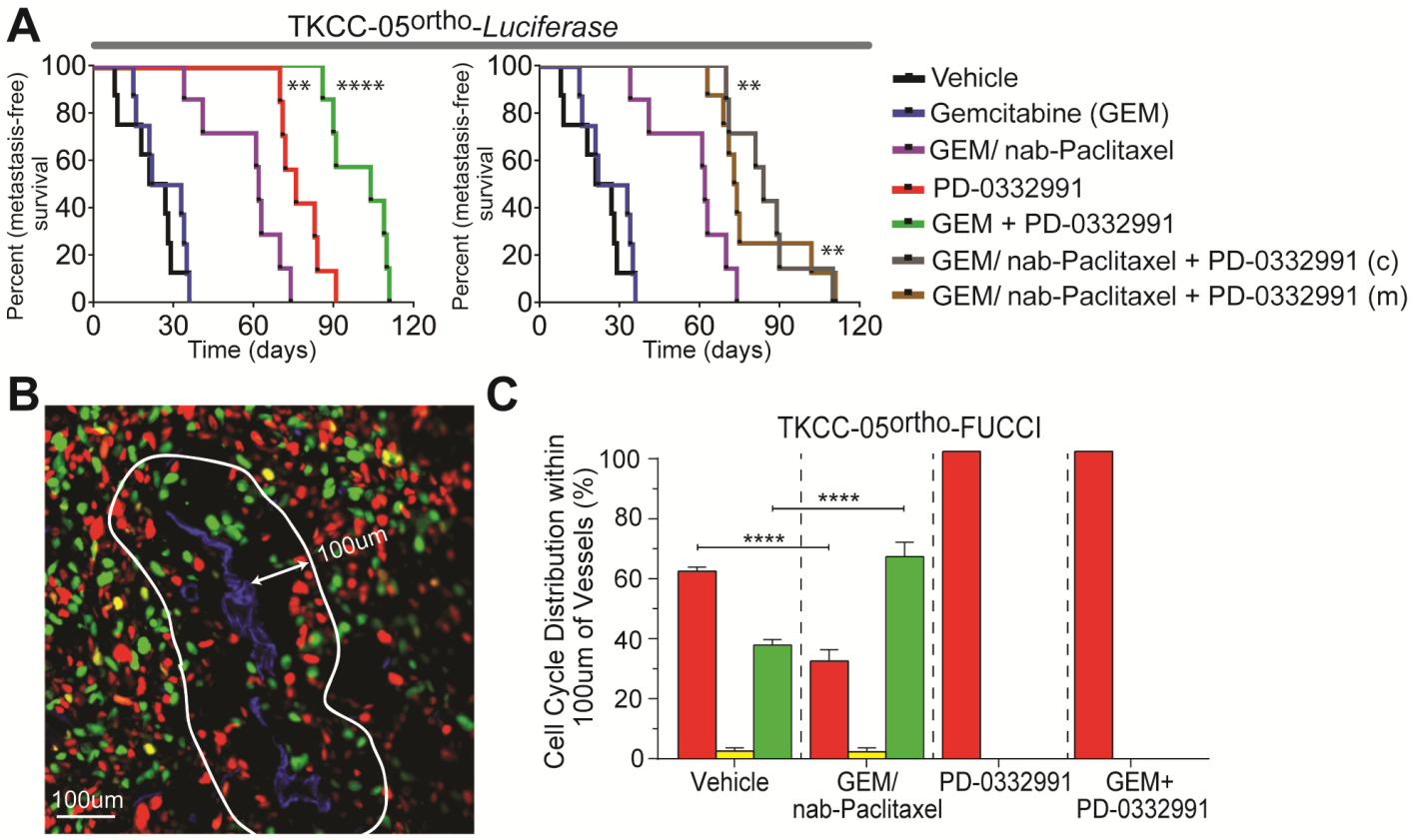

Supplementary Figure S13. PD-0332991-based treatment and combinations significantly improved metastasis-free survival in RB-high PDA, inducing effective cell cycle arrest. **(A)** Briefly, 15,000 luciferase-labeled PDCLs were injected into the pancreas of 6-8 week old Nod/Scid/IL-2Rγnull (NSG) mice. Mice were randomized into treatment groups at one week post-injection, with two additional treatment arms included, involving triple combination of gemcitabine (70mg/kg), nab-Paclitaxel (30mg/kg) twice weekly IP administered either concomitantly with PD-0332991 (100mg/kg) gavage from week 2 on a 5-day "on", 5-day "off" schedule for 20 days (concomitant; (c)), or with PD-0332991 administered as maintenance therapy by daily gavage after completion of gemcitabine/nab-Paclitaxel treatment (m). Tumor burden was monitored weekly by bioluminescent imaging until ethical endpoint. Kaplan-Meier metastasis-free survival analyses of PD 0332991 monotherapy, in combination with gemcitabine (GEM; *left*) or triple combinations with GEM/nab-Paclitaxel (*right*), compared with GEM/nab-Paclitaxel. **(B)** Representative pancreas tissue section from a vehicle treated mouse injected orthotopically with TKCC-05-FUCCI cells. CD31 staining indicated in blue. Cells within 100µm of a vessel were counted using ImageJ2 software (100µm margin indicated by white line). **(C)** Cell cycle distribution within the 100µm boundary was quantified for vehicle, GEM/nab-Paclitaxel, PD-0332991 and GEM+PD-0332991 treatment groups. (*n*=4 mice per treatment group, data shown as mean ± SEM).

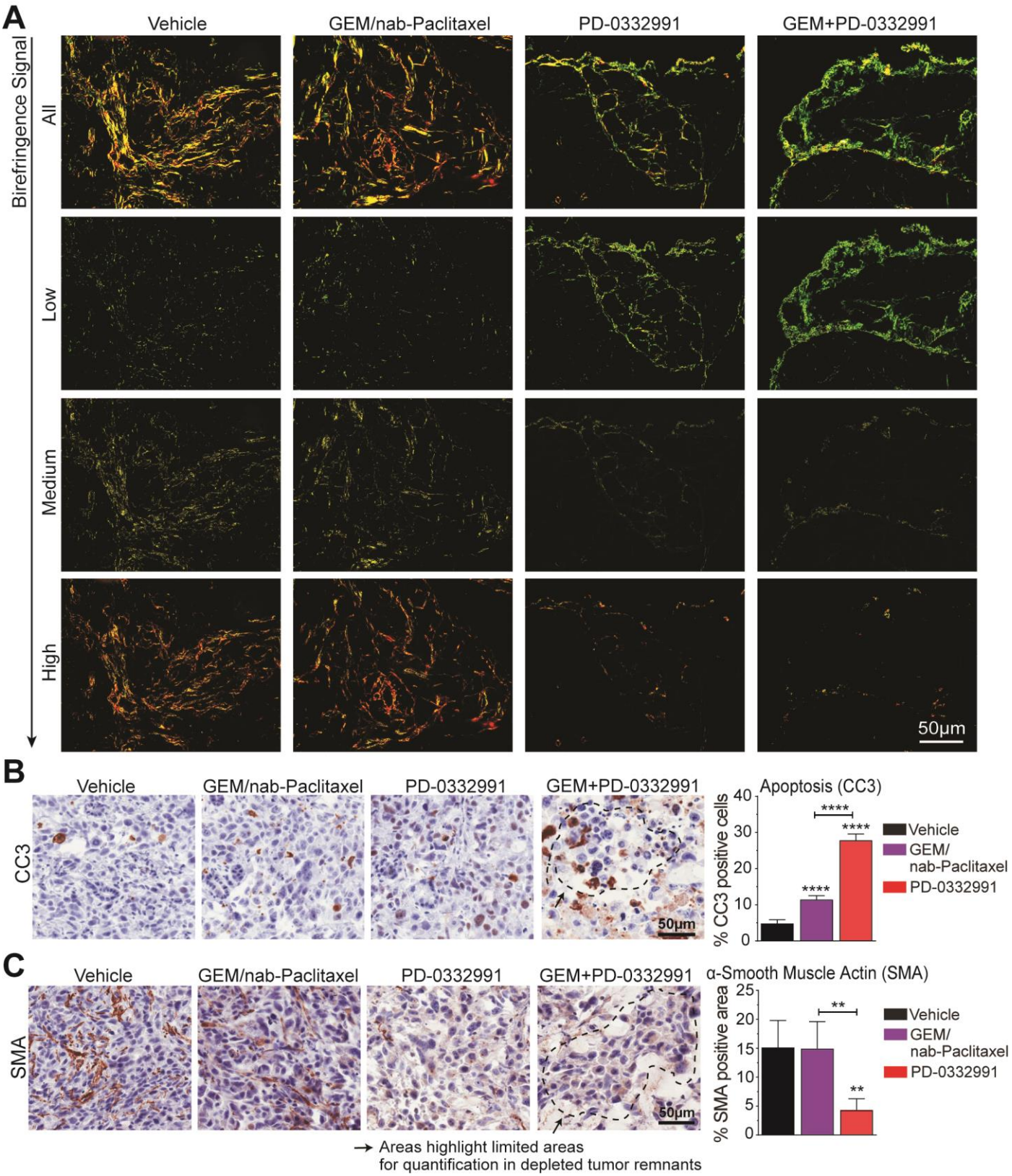

Supplementary Figure S14. PD-0332991-based therapeutic interventions alter key signaling events within the tumor microenvironment of an RB-high orthotopic patient-derived model of PDA. **(A)** Representative images of signal emitted from collagen fibres with high (red/orange), medium (yellow), and low (green) birefringence in tumor tissue following different treatments, imaged with polarized light microscopy. Representative images and quantification of **(B)** cleaved caspase 3 staining as a marker of apoptosis and **(C)** α-smooth muscle actin (SMA) expression in the same tissues. Data shown as mean ± S.D. (*n*=4 animals per treatment group were used for analysis). GEM+PD-0332991 tumor remnants contained insufficient areas of viable cells for quantification in these sets of experiments due to sectioning for previous analyses.

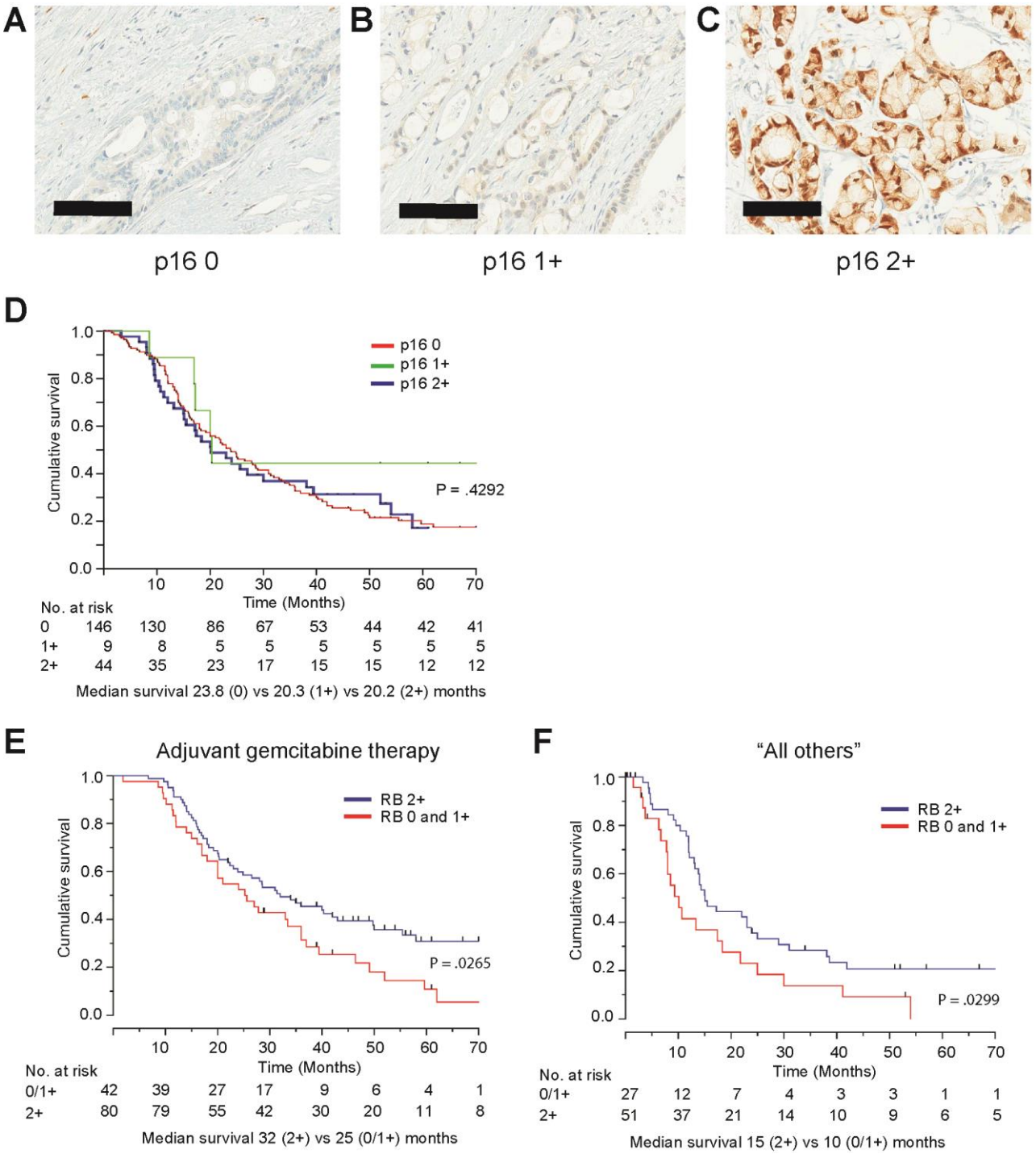

Supplementary Figure S15. Cumulative survival analysis of patients with PDA based on p16 immunohistochemistry. Example of **(A)** p16-negative tumor (0); **(B)** Weakly p16-positive tumor (1+) and **(C)** Tumor with strong nuclear p16 staining (2+). *Scale bar* = 100µm. **(D)** Kaplan-Meier analyses of disease-specific survival based on p16 immunohistochemistry. Significance was examined using Log-rank test comparing disease-specific survival in all three p16 groups revealed no significant difference (P=0.7703). Kaplan-Meier analyses of disease-specific survival based on RB immunohistochemistry (RB high vs RB low) examined based on adjuvant treatment: **(E)** 122 patients who completed 6 cycles of adjuvant gemcitabine and **(F)** "all others" group which included 78 patients who received no adjuvant therapy or other chemotherapies.